A THEORETICAL TREATMENT OF SOLVENT EFFECTS

BY

SHAHUL HAMEED M. NILAR

A DISSERTATION PRESENTED TO THE GRADUATE SCHOOL
OF THE UNIVERSITY OF FLORIDA IN PARTIAL FULFILLMENT
OF THE REQUIREMENTS FOR THE DEGREE OF
DOCTOR OF PHILOSOPHY

UNIVERSITY OF FLORIDA

1989

In memory of my

father

and

brother.

ACKNOWLEDGEMENTS

For suggesting the topic of this dissertation, all the discussions and help in pursuing my interests in solvation, I wish to thank my research director Dr. Michael Zerner.

A belated word of thanks goes to Dr. Serafin Fraga of The University of Alberta, Canada, for introducing me to the theory of intermolecular interactions. His directness in dealing with all matters was indeed a source of inspiration to me. None of this work would have been possible if not for the tireless efforts of Dr. Ranjit Thuraisingham of Macquarrie University, Australia, who taught me quantum chemistry in his unique manner — through kindness and patience. I will always be indebted to him.

Special thanks go to Dr. David Micha of the University of Florida for two challenging courses in intermolecular interactions and advanced kinetics. I have learned a tremendous amount from him. Dr Osiel Bonfim's help with the statistical mechanics in this work is gratefully acknowledged. The discussions I had with him helped me immensely.

To Ms. Margaretha Micha is due a very sincere thank you for listening to me and helping me through some of the most emotionally difficult times.

TABLE OF CONTENTS

page

ACKNOWLEDGEMENTS iii

ABSTRACT vi

CHAPTERS

1 INTRODUCTION 1

2 SPECTRAL SHIFTS USING THE CONTINUUM MODEL FOR THE SOLVENT 8

2.1 Introduction 8
2.2 Derivation of Equation for the Interaction Energy ΔE 10
2.3 Parameterisation of the Expression for ΔE 15
2.4 Variation of a Trial Solute Wavefunction Ψ' in the Presence of the Continuum Solvent 19
2.5 Determination of the Cavity Radius 'a' 23
2.6 Results of calculations and discussions 24
2.7 Conclusions 31

3 SEARCH FOR THE GLOBAL MINIMUM ON A POTENTIAL ENERGY SURFACE 34

3.1 Introduction 34
3.2 The Simulated Annealing Method 36
3.3 Choice of Potential Energy Function 39

3.4 Results and Discussion of the Simulated Annealing Method 50
3.5 Discussion. 67

4 ELECTRONIC SPECTRA USING THE DISCRETE-CONTINUUM SOLVENT MODEL. 70

4.1 Introduction 70
4.2 Derivation of the Hamiltonian for the Solute-Discrete Solvent System. 71
4.3 Electronic Spectra of a Solute with a Discrete Number of Solvent Molecules. 73
4.4 Shifts in the Electronic Spectra of a Solute using the Discrete-Continuum Model 83
4.5 Conclusions. 86

5 AN ALGORITHM FOR THE MORE REALISTIC DESCRIPTION OF THE SOLUTE MOLECULE. 88

5.1 Introduction 88
5.2 Mathematical Formulation of the Algorithm 88
5.3 Results and Discussion of the Applications of the Point Charge Model. 92

6 CONCLUSIONS 98

APPENDIX THE REACTION FIELD METHOD. 102

REFERENCES 107

BIOGRAPHICAL SKETCH 112

Abstract of Dissertation Presented to the Graduate School
of the University of Florida in Partial Fulfillment of the
Requirements for the Degree of Doctor of Philosophy

A THEORETICAL TREATMENT OF SOLVENT EFFECTS

By

SHAHUL HAMEED M. NILAR

May, 1989

Chairman : Dr. M. C. Zerner
Major Department: Chemistry

Most chemical reactions take place in solution and, in order to understand the molecular processes that take place during reaction, it is necessary to include the effect of the surrounding medium on the reacting species. As the solvent is usually in molar quantities, it is impossible to study an Avagadro's number of molecules using the principles of quantum mechanics. To overcome this difficulty, reasonable models that adequately describe the solvent have to be constructed.

Three such models are presented in this thesis. The first describes the solvent as a continuum with the solute molecule centered in a spherical cavity embedded in the solvent. This model does not assign a structure to the molecules in the solvent. The second model builds a cluster of solvent molecules around the solute using the method of simulated annealing, a method based on the Metropolis Monte Carlo algortihm. The specific nature of the interactions between the solute and solvent molecules is taken into consideration in this method.

The third model uses the second model to build a cluster of solvent molecules around the solute and this entire solute-solvent cluster is then enclosed in a spherical cavity and embedded in the solvent.

Solvent induced spectral shifts in solute molecules were evaluated using the first and third models and the results obtained compared with experimental shifts. The method used to calculate the shifts was the Intermediate Neglect of Differential Overlap which has been parameterized for the study of spectral transitions.

Not all molecules can be described, even approximately, by a spherical cavity model. An algorithm is presented that defines a more realistic shape for this cavity as a set of interlocking spheres centered on the atoms of the solute. The results of the application of this method to such processes as molecular dissociation are also presented.

CHAPTER 1
INTRODUCTION

Solvation is the process in which one system, usually at a lower concentration, interacts with another system, which is in larger amounts. The first system is referred to as the solute and the latter is termed the solvent. The interaction between the two systems can affect the structure of the constituent molecules. Consequently, the chemical and physical properties of these molecules show a change from their corresponding values in the gas phase or vacuum.

An exact numerical study of solvent effects, based on the principles of quantum mechanics is impossible, even after the advent of supercomputers as the number of electrons and nuclei which constitute the interacting molecules are of the order of Avogadro's number. Even an approximate theory for such a number of particles is questionable, as the simplifications would have to be drastic, thereby making the interpretation of the results difficult.

In order to overcome this difficulty, models that adequately represent the solvent have to be constructed and then incorporated into the quantum mechanical description of the solute system (1). The validity of these models is usually checked by evaluating thermodynamic properties like the specific heats and isothermal compressibility, and comparing these results with experiment.

Solvent models can be broadly classified into one of the following categories:

1. Continuum models
2. Discrete models.

A synthesis of the two, referred to as the discrete-continuum approach, incorporates the positive aspects of each model for a better description of the solvent.

In the continuum model, the solute molecule is represented by a point dipole centered in a cavity which is embedded in the solvent. The shape of this cavity can be chosen beforehand and usually is taken to be a sphere, ellipsoid or a rod-like tube. The solvent is described as a continuous medium with a specific dielectric constant (ϵ) and an associated refractive index (n). Clearly, this description does not take the structure of the solvent molecules into account.

The specific nature of the solute-solvent interactions is important, particularly in the case of polar species. The dipolar interactions are most important in ordering the solvent molecules around the solute to form solvation shells. The properties of the molecules in these shells are quite different from those in the bulk areas of the solvent. By using the same value for the dielectric constant, the specific nature of the solute solvent interactions is neglected.

Beveridge and Schnuelle (2) attempted to include a solvation shell within the continuum model by centering the point dipole inside two concentric spheres. The value of the dielectric constant for the solvent between the two spheres is different from that of the bulk solvent which is outside the second sphere. The major

shortcomings in this model are the choice of values for the dielectric constants and the radii defining the spheres, which are arbitrary.

Surrounding the solute with a suitable number of solvent molecules is the basis of the discrete model. The number of such molecules is chosen based on intuition and prior experience. Studies on such solute-solvent complexes explicitly include the anisotropic nature of the associated interactions. However, the disadvantage in using this scheme is the choice of an adequate number of solvent molecules that accurately describe the solvent. For typical dipolar cases, this number can be in the thousands which makes a meaningful numerical treatment impossible.

The solvent model of Noell and Morokuma (3) is obtained from good ab-initio calculations on supermolecular complexes. The atoms in the solvent molecules are then replaced by fractional point charges which are chosen to reproduce the interaction energy calculated for the complex. The drawbacks in this approach are that a prior knowledge of the solvent structure is required and the effects of the bulk solvent are now neglected.

A natural extension of the two models described above is the discrete-continuum approach. Based on a suitable theoretical formulation, the solute is surrounded by a predetermined number of solvent molecules and the resulting system, which now consists of explicit solvation shells, is then embedded in the fluid continuum. The quantum mechanical study of the solvated complex within the discrete model can be achieved using the following methods:

1. Variation scheme.

2. Perturbational treatment.

In the former case, the solvated complex is treated as one molecule referred to as a supermolecule. The interaction energy ΔE of the solute molecule A with the N surrounding solvent molecules B_i, {i=1,2, ..., N} is calculated as

$$\Delta E = E_{AB_1B_2...B_N} - \left\{ E_A + \sum_{i=1,N}^{N} E_{B_i} + E_{B_1B_2...B_N} \right\} \qquad 1.1$$

The first term on the right hand side of the above equation is the energy of the supermolecule. E_A and E_{Bi} are the energies of the solute and the i^{th} solvent molecule respectively. The last term in the equation is the solvent — solvent interaction energy. These energies are usually calculated in the Hartree-Fock scheme using a finite basis set. Clearly, the supermolecule approach is practical only when the size of the solute and the number of solvent molecules are very small, and, even in such cases, the choice of the basis set is very important in obtaining meaningful results (4). The numerical accuracy required in determining each of the terms on the right hand side of the equation (1.1) has to be extraordinarily high as the interaction energy is obtained by subtraction.

If the solvent induced structural changes in the solute are considered to be small, a perturbational scheme seems to be more suitable in studying intermolecular interactions. Using the theory of weak interactions, the energy of interaction ΔE can be expanded in a multipolar series expressed as a function of the inverse of the distance separating the systems (5). An advantage in such a formalism is that each term in the series has a physical meaning, such as the coulombic,

induced energy contributions, etc. This generalized multipolar expansion is an infinite series and for reasons of computational efficiency has to be truncated after a suitable number of terms. The coefficients of each of the remaining terms are determined by fitting the expansion to experimental thermodynamical quantities (6) or values of the interaction energy obtained for model systems from good ab-initio calculations (7).

After the multipolar expansion for ΔE has been defined, the interaction energy for the solute-solvent cluster can be evaluated. The number of solvent molecules in such a cluster can be determined by calculating the interaction energy per solvent molecule, ΔE_1 for an increasing number of solvent molecules (m) around the solute. The value of m at which ΔE_1 converges, within a predetermined value, is chosen to be the number of solvent molecules in the solvation shell. The solvated complex is then centered in a cavity of suitable dimensions and emersed in the continuum fluid. In this way, the anisotropy in the solvent shells and the interactions due to the bulk fluid can be accounted for.

Shifts in the electronic spectra of molecules due to solvation is the main area of research presented in this dissertation. Certain dyes can have different colors depending on the nature of the solvent they are in. An example is 4–nitro – 4′ – (N,N diethyl) diazabenzene (Figure 1.1) which is yellow-orange in cyclohexane and deep red in ethanol.

Empirical rules have been proposed (8,9) to calculate these shifts. Although these rules are helpful in predicting the positions of spectral peaks in various sol-

vents to within 5 to 10 nm of experiment, they offer no insight into the molecular processes that cause these shifts. An understanding of these interactions should be based on good microscopic concepts.

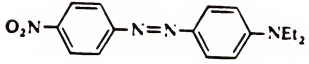

Figure 1.1 Structure of 4–nitro – 4′– (N,N diethyl) diazabenzene.

In order to study the origin of such spectral shifts, the three solvent models described above were used. In each case the effective nature of the surroundings was incorporated into the Hamiltonian of the solute. The solute Hamiltonian is obtained from the Intermediate Neglect of Differential Overlap (INDO) approximation (10) to the Hartree-Fock self-consistent field equations (11) as parameterized by Ridley and Zerner (12) and Bacon and Zerner (13), but the methods developed are not limited to this model.

Chapter two of this thesis introduces the partitioning of the solute–solvent system. The solvent is treated as a continuum and the mathematical formulation for the calculations derived. The values calculated for the shifts in the spectral peaks for a series of molecules in various solvents are tabulated.

Obtaining the discrete solvent strucure is the main focus of the theory outlined in Chapter 3. The theory of the Simulated Annealing method (14) and the results obtained for the solvation of neutral molecules and ions are presented.

The structures obtained for the solvent clusters using the method described in chapter three are replaced by point charges having the same values as those used in the simulation. The spectral shifts in such clusters are calculated and compared with the corresponding experimental values obtained from laser jet studies. These solute-solvent clusters are then embedded in the continuum solvent. The theory used to calculate the shifts within the discrete-continuum model along with the results obtained are presented in Chapter 4.

An algortihm which defines a more realistic shape of the molecular cavity in the solvent as a set of interlocking van der Waals spheres centered on the atoms of the solute is presented in Chapter 5. The effect of the image charges induced by the solute on the surface of the cavity is incorporated into the solute Hamiltonian. Processes like molecular dissociation are studied and the results tabulated.

The last chapter gives the conclusions reached on the use of the methods presented in this thesis. The advantages and shortcomings in the methods and the parameterization are outlined, along with possible extensions for the future.

CHAPTER 2
SPECTRAL SHIFTS USING THE CONTINUUM MODEL FOR THE SOLVENT

2.1 Introduction

The configuration space spanned by the solute and the solvent can be partitioned into three subspaces — one that is described by the electrons and nucleii of the solute S, the second subspace D, that is spanned by the discrete solvent molecules immediately surrounding the solute, and the continuum solvent space C, described by the dielectric constant (ϵ) and the refractive index (n). As the solvent induced changes in the properties of the solute are considered to be small, the effect of the solvent can be written as a perturbational expansion in the parameter λ. The Hamiltonian H'_S for the solvated complex can now be written as

$$H'_S = H_S + \lambda H^{(1)}_{S-D} + \lambda^2 H^{(2)}_{S-D} + \lambda^3 H^{(3)}_{S-D} + \ldots$$

$$+\lambda H^{(1)}_{S-C} + \lambda^2 H^{(2)}_{S-C} + \lambda^3 H^{(3)}_{S-C} + \ldots + \Delta \qquad 2.1$$

where $H_{I,J}$, I,J ϵ {S, D, C} is the Hamiltonian for the interaction between the subspaces I and J and H_S describes the quantum mechanics of the solute. Δ represents the interaction between the continuum and discrete subspaces, and each of these with itself.

In this chapter, the solvent induced shifts in the electronic spectra of a series of molecules are calculated. The solvent is treated as a continuum; that is, the

coupling between the solute space and discrete solvent space is neglected. As the time elapsed during electronic transitions is of the order of 10^{-18} seconds, changes in the solvent structure that effect the interactions within the solvent can be neglected. Thus, Δ is assumed to be the same for the ground and excited states of the solute and need not be considered explicitly in the formulation. The approximate Hamiltonian H''_S for the solvated complex is now given by

$$H''_S = H_S + \lambda H^{(1)}_{S-C} + \lambda^2 H^{(2)}_{S-C} + \lambda^3 H^{(3)}_{S-C} + \ldots \qquad 2.2$$

Expressions for the solute-solvent interaction are derived based on the theory of weak interactions and the energy of interaction is then parameterized using the reaction field theory of Onsager (15). These derivations are given in sections 2.2 and 2.3 respectively.

The Intermediate Neglect of Differential Overlap (INDO) method (10) has been particularly useful in the prediction of electronic spectra. This method, as parameterised by Ridley and Zerner (12) and Bacon and Zerner (13) is used to describe the solute molecule. The formulation of the method is well documented and will not be repeated here.

The incorporation of the effective solvent Hamiltonian and derivation of the wavefunction of the solute (in the solvent) is presented in section 2.4, the restrictions on the wavefunction during the variation are the orthonormality requirement and the reaction field energy derived in section 2.3.

The Onsager model treats the solute molecule as a point dipole centered in a cavity. The shape of the cavity chosen here is a sphere and the methods used to evaluate the radius of this cavity are discussed in section 2.5

Section 2.6 gives the calculated and experimental spectral shifts for a series of molecules in various solvents. The final section gives the conclusions reached from this study and criticisims of the continuum model.

2.2 Derivation of Equation for the Interaction Energy ΔE

When the distance separating two interacting systems A and B is larger than their individual dimensions, the supermolecular system can be studied using the theory of weak interactions. Neglecting the permutation of electrons between the systems is justified on the basis of the large intersystem distance and the wavefunction of the composite system Ψ can be approximated as the simple product of the wavefunctions of the individual systems Ψ_A and Ψ_B as

$$\Psi = (A_A\Psi_A)(A_B\Psi_B)$$

where A_A and A_B are the antisymmetrizers for the electrons in systems A and B respectively.

In the following derivation, the solute whose spectrum is to be studied is denoted by A, while the N solvent molecules surrounding it, which comprise system B, will be referred to as $B_1, B_2, \ldots, B_N$. Let α and β refer to the nuclei and a, b to the electrons of systems A and B_k, { k = 1, 2, . . ., N } respectively.

Further, let these particles have coordinates r_α, r_β, r_a and r_b relative to origins O_A and O_{Bk} with the distance O_AO_{Bk} being equal to R_k.

The Hamiltonian H for the supermolecular system AB_k can be written as

$$H = H_A + H_{B_k} + H_{AB_k} \qquad 2.3$$

where H_I, (I = A, B_k) and H_{ABk} are the Hamiltonians for system I and the interaction between A and B_k respectively. H_{ABk} can be written in the usual manner as

$$H_{AB_k} = \sum_{\alpha<\beta} \frac{Z_\alpha Z_\beta}{r_{\alpha\beta}} - \sum_{I=\alpha}\sum_{i=b} \frac{Z_I}{r_{Ii}} - \sum_{I=\beta}\sum_{i=a} \frac{Z_I}{r_{Ii}} + \sum_{a<b} \frac{1}{r_{ab}} \qquad 2.4$$

Z_I (I = α, β) is the charge on the nucleus I. The distance r_{MN} between particles M and N, where M,N can be nucleii or electrons is given by

$$r_{MN} = R\{1 + 2\frac{(z_N - z_M)}{R}$$

$$+\frac{(x_N - x_M)^2 + (y_N - y_M)^2 + (z_N - z_M)^2}{R^2}\}^{\frac{1}{2}} \qquad 2.5$$

If the two systems A and B_k are electronically neutral, equation (2.5) substituted in equation (2.4) yields, after manipulation, a leading term in R^{-3} as the R^{-1} and R^{-2} terms disappear. Defining the dipole moment operators M^A and M^{B_k} of systems A and B_k as

$$M^A = \sum_{\alpha \in A} Z_\alpha r_\alpha - \sum_{a \in A} r_a$$

$$M^{B_k} = \sum_{\beta \in B_k} Z_\beta r_\beta - \sum_{b \in B_k} r_b$$

H_{ABk} can be written as

$$H_{AB_k} = R^{-3} M^A \Theta^{AB_k} M^{B_k} + O\left(R^{-4}\right) \qquad 2.6$$

where Θ^{AB_k} is the orientation tensor between A and B_k. The Hamiltonian H_{AB} for the solute molecule in the presence of the N solvent molecules is now given by

$$H_{AB} = H_A + \sum_{k=1}^{N} \left(H_{B_k} + H_{AB_k}\right) \qquad 2.7$$

Equations (2.6) and (2.7) indicate that the leading term of the interaction is the dipole-dipole term.

Evaluation of the interaction energy ΔE by treating the interaction Hamiltonian H_{AB} as a perturbation requires the definition of a reference wavefunction for the solute-solvent complex. To evaluate the second order interaction energy, excited state wavefunctions for the solvated complex need to be defined. From equation (2.7), it is clear that H_{AB} involves a summation over the solvent molecules B_k, one molecule at a time. It is therefore necessary to consider only those excited state wavefunctions in which the solute molecule and/or one solvent molecule is excited.

Assuming that the solute and solvent molecules are far apart, the wavefunctions for the solvated solute system in the weak interaction limit are

$$\Psi_0 = \psi^0_A \psi^0_{B1} \psi^0_{B2} \ldots \psi^0_{Bk} \ldots \psi^0_{BN} \qquad 2.8a$$

$$\Psi_1 = \{\psi^e_A \psi^0_{B1} \psi^0_{B2} \ldots \psi^0_{Bk} \ldots \psi^0_{BN}\} \qquad 2.8b$$

$$\Psi_2 = \{\psi^0_A \psi^0_{B1} \psi^0_{B2} \ldots \psi^b_{Bk} \ldots \psi^0_{BN}\} \qquad 2.8c$$

$$\Psi_3 = \{\psi^e_A \psi^0_{B1} \psi^0_{B2} \ldots \psi^b_{Bk} \ldots \psi^0_{BN}\} \qquad 2.8d$$

In equations (2.8 a-d), ψ^0_A and ψ^0_{Bk} are the wavefunctions for the solute molecule and the k^{th} solvent molecule in the ground state (denoted 0). The excited state wavefunctions for these molecules are denoted by ψ^e_A and ψ^b_{Bk} respectively. $\Psi_I = \{\ \}$, I=1, 2, 3, represents the set of all possible inferred excitations.

The first order change in the energy $E^{(1)}$ due to the solute–solvent interaction H_{AB} is given by

$$E^{(1)} = < \Psi_0 | H_{AB} | \Psi_0 >$$

Substituting equation (2.8a) in the above equation and using the definitions of the dipole moment operators M^A and M^{B_k} given before

$$E^{(1)} = \sum_{p=1}^{N} R_p^{-3} \mu^0_A \Theta^{AB_p} \mu^0_B \qquad 2.9$$

where μ^j_I (I=A, B ; j = 0, e, b) is the dipole moment of system I in state j.

$E^{(2)}$, the second order change in the energy, is given by

$$E^{(2)} = -\sum_{l=1}^{3} \frac{| < \Psi_0 | H_{AB} | \Psi_l > |^2}{(E_l - E_0)} \qquad 2.10$$

where the wavefunctions Ψ_l, l = 1, 2, 3, have been defined in equations (2.8b — d). Defining the polarisability tensor $\alpha^0{}_A$ of A in state 0 as

$$\alpha^0_A = 2\sum_{\epsilon\neq 0} \frac{|<\psi^0_A|M^A|\psi^\epsilon_A>|^2}{(E^\epsilon_A - E^0_A)} \qquad 2.11$$

the second order contribution to the energy from wavefunction Ψ_1 is given by

$$E^{(2)}_1 = -\frac{1}{2}\sum_{p,q=1}^{N} R_p^{-3}R_q^{-3}\mu^0_{B,p}\Theta^{AB_p}\alpha^0_{B,p}\Theta^{AB_q}\mu^0_{B,q} \qquad 2.12$$

Similarly, the contribution $E_2{}^{(2)}$ from Ψ_2 is

$$E^{(2)}_2 = -\frac{1}{2}\sum_{p=1}^{N} R_p^{-6}\mu^0_A\Theta^{AB_p}\alpha^0_B\Theta^{AB_q}\mu^0_A \qquad 2.13$$

where the polarisability tensor of B is defined analogous to equation (2.11).

$E_3{}^{(2)}$ which is defined as

$$E^{(2)}_3 = -\frac{|<\Psi_0|H_{AB}|\Psi_3>|^2}{(E_3 - E_0)}$$

is the energy due to the interaction of the excited states of the solute and solvent molecules and this term is the dispersion energy contribution to the second order energy. In the method presented here, the explicit form of this term will be neglected and will henceforth be denoted as D_g.

The change in energy ΔE of the solute, to second order, can now be written as

$$\Delta E = E^{(1)} + E^{(2)}_1 + E^{(2)}_2 + D_g \qquad 2.14$$

where the terms on the right hand side of the above equation have been defined in equations (2.9), (2.12) and (2.13).

Each of the terms in equation (2.14) is calculated as a sum over the N solvent molecules. When the number of such molecules is of the order of Avagadro's number, such summations are not practical and have to be replaced by statistical mechanical averages over all the configurations of the solvent molecules, leading then to macroscopic parameters.

2.3 Parameterization of the Expression for ΔE

The reaction field theory of Onsager (15) treats the solvent as a continuum and the inherent assumption is that the solvent is isotropic. In other words, no molecular structure is assigned to the solvent. Thus, the polarisability tensors in the above equations can be replaced by their corresponding scalar values. As the solvent lacks a structure, the summations in these equations, which are over the number of solvent molecules, are replaced by statistical averages in terms of macroscopic properties like the dielectric constant (ϵ) and the refractive index (n).

The solute is treated as a polarizable dipole centered in a cavity which is embedded in the continuum. For purposes of simplicity, the cavity is assumed to be a sphere of radius 'a'. The solute dipole μ^0_A creates an image dipole in the opposite direction in the solvent. This image dipole, in turn, augments the solute dipole and creates a uniform field called the reaction field, $\boldsymbol{R}$, which enhances the already existing field in the cavity.

The reaction field $\boldsymbol{R}$ is given by (15)

$$R = \frac{2(D'-1)}{a^3(2D'+1)}\mu^0_A \qquad 2.15$$

where D′ is that part of the static dielectric constant which takes the interactions between the solute dipole and the permanent dipoles of the solvent molecules into account. The derivation of this equation is given in the Appendix.

Let

$$f = \frac{2(D' - 1)}{a^3(2D' + 1)}$$

For a polarizable solute dipole μ^0_A with isotropic polarizability α, the reaction field $\boldsymbol{R}$ is given by

$$R = f\left(\mu^0_A + \alpha R\right) \qquad 2.16$$

Approximating α by $a^3/2$ (16), the reaction field for a polarizable solute is now given by

$$R = \frac{2}{a^3}\left(\frac{D' - 1}{D' + 2}\right)\mu^0_A \qquad 2.17$$

The static dielectric constant ϵ of the solvent is comprised of two parts, one due to the permanent dipole orientation D′ and the other D″, due to the electronic polarizability of the solvent (17,18). The latter contribution can be evaluated using the Maxwell relation $D'' = n^2$, where n is the refractive index of the solvent.

The dielectric term in the above equation can be calculated using the following relation:

$$\frac{D' - 1}{D' + 2} = \frac{\epsilon - 1}{\epsilon + 2} - \frac{n^2 - 1}{n^2 + 2} \qquad 2.18$$

Substituting equation (2.18) in (2.17) yields

$$R = \frac{2}{a^3}\left\{\frac{\epsilon - 1}{\epsilon + 2} - \frac{n^2 - 1}{n^2 + 2}\right\}\mu_A^0 \qquad 2.19$$

Analysis of equation (2.9) shows that the first order term $E^{(1)}$ is due to the coupling of the solute dipole with the permanent dipoles of the solvent which is exactly the reaction field $\boldsymbol{R}$. Therefore, taking the statistical average over the solvent molecules, the term $E^{(1)}$ in equation (2.14) can be written as

$$E^{(1)} = -\mu_A^0 R \qquad 2.20$$

where $\boldsymbol{R}$ is given by equation (2.19).

In a similar manner, the second term on the right hand side of equation (2.14) is the coupling of the field due to the permanent solvent dipoles with the polarizability tensor of the solute. This term can be written as (19)

$$E_1^{(2)} = -\frac{1}{2}\sum_{p,q=1}^{N} R_p^{-3} R_q^{-3} \mu_{B,q}^0 \alpha_A^0 \mu_{B,p}^0 \qquad 2.21$$

The field at the p^{th} solvent molecule due to the permanent dipole of the solute is represented by the third term of equation (2.14). As in the previous case,

$$E_2^{(2)} = -\frac{1}{2}\sum_{p=1}^{N} R_p^{-6} \alpha_{B,p}^0 \left(\mu_A^0\right)^2 \qquad 2.22$$

where $\alpha^0{}_p$ is the static polarizability of the p^{th} solvent molecule. Equation (2.22) represents the induction energy due to the polarization of the solvent by the permanent solute dipole.

Averaging the terms in equation (2.22) over the molecular orientations, the reaction field r at the p^{th} solvent molecule due to the induction effects of the permanent dipole of the solute molecule is given by

$$r = \frac{2}{a^3}\left(\frac{n^2-1}{n^2+2}\right)\mu_A^0 \qquad 2.23$$

where n is the refractive index of the solvent.

Thus, ΔE is now given by

$$\Delta E = -\mu_A^0 R - \frac{1}{2}\sum_{p,q=1}^{N} R_p^{-3} R_q^{-3} \mu_{B,q}^0 \alpha_A^0 \mu_{B,p}^0$$

$$-\left(\frac{n^2-1}{n^2+2}\right)(\mu_A^0)^2 + D_g \qquad 2.24$$

The time scales for electronic excitations are of the order of 10^{-18} seconds, about a million times faster than the vibrational motion of the nuclei. When the solute molecule is excited, its dipole is altered and the dipoles of the solvent molecules will change in order to accommodate this effect. The reorientation of the permanent part of the solvent dipole can be neglected as the nuclei are assumed to be fixed during the electronic transition. Thus, the excitations considered obey the Frank-Condon principle. However, the electronic part of the dipole moment will change, and this effect is taken into consideration by using the reaction field term which depends on the refractive index of the solvent, namely equation (2.23).

For the excited state of the solute with a dipole moment μ^e_A, the change in energy ΔE_{ex} due to solvation is given by

$$\Delta E_{ex} = -\frac{\mu^e_A \cdot \mu^0_A}{a^3}\left\{\frac{2(\epsilon-1)}{(\epsilon+2)} - \frac{2(n^2-1)}{(n^2+2)}\right\}$$

$$-\frac{(\mu^e_A)^2}{a^3}\left(\frac{n^2-1}{n^2+2}\right) - \frac{1}{2}\sum_{p,q=1}^{N} R_p^{-3} R_q^{-3} \mu^0_{B,q} \alpha^e_A \mu^0_{B,p} - D_e \qquad 2.25$$

where D_e is the dispersion energy term for the excited state of the solute. The shift in the spectral peak $\Delta\nu$ due to solvation can now be calculated from equations (2.24) and (2.25) as

$$\Delta\nu = \Delta E - \Delta E_{ex} \qquad 2.26$$

2.4 Variation of a Trial Solute Wavefunction Ψ' in the Presence of the Continuum Solvent

Let

$$g = \frac{2}{a^3}\left\{\frac{2(\epsilon-1)}{\epsilon+2} - \frac{n^2-1}{n^2+2}\right\} \qquad 2.27$$

and

$$H^* = H_s - \frac{1}{2}\hat{\mu}^T . g . \hat{\mu} \qquad 2.28$$

where H^* and H_s are the Hamiltonian operators for the solute molecule in the solvent and gas phase respectively and μ is the total dipole moment operator. The superscript T denotes the transpose.

Define a function L according to

$$L = E - \lambda \left[< \Psi' | \Psi' > -1 \right]$$

$$+\frac{\gamma}{2}\{ < \Psi' | \hat{\mu}^T | \Psi' > .g. < \Psi' | \hat{\mu} | \Psi' > -g \left(\mu_A^0 \right)^2 \}$$

where λ and γ are constants to be determined and Ψ' is the normalized trial wavefunction for the solute in the solvent. $\mu^0{}_A$ is the expectation value of the operator μ for the wavefunction Ψ. E is the energy of the solute molecule in the presence of the continuum solvent and is given by

$$E = < \Psi' | H^* | \Psi' >$$

Using variational theory

$$\delta L = < \delta\Psi' | H^* | \Psi' > + < \Psi' | H^* | \delta\Psi' >$$

$$-\lambda \left[< \delta\Psi' | \Psi' > + < \Psi' | \delta\Psi' > \right]$$

$$+\frac{\gamma}{2}\{ < \delta\Psi' | \hat{\mu}^T | \Psi' > .g. < \Psi' | \hat{\mu} | \Psi' > \qquad 2.29$$

$$+ < \Psi' | \hat{\mu}^T | \Psi' > .g. < \delta\Psi' | \hat{\mu} | \Psi' >$$

$$+ < \Psi' | \hat{\mu}^T | \Psi' > .g. < \Psi' | \hat{\mu} | \delta\Psi' >$$

$$+ < \Psi' | \hat{\mu}^T | \delta\Psi' > .g. < \Psi' | \hat{\mu} | \Psi' > \}$$

At a stationary point $\delta L = 0$. As μ is a hermitian operator,

$$< \Psi' | \hat{\mu}^T | \Psi' > = < \Psi' | \hat{\mu} | \Psi' >$$

Collecting terms, equation (2.29) reduces to

$$0 = < \delta\Psi' | H^* - \lambda + \gamma g \left(\mu_A^0\right)^2 | \Psi' >$$

$$+ < \Psi' | H^* - \lambda + \gamma g \left(\mu_A^0\right)^2 | \delta\Psi' > \qquad 2.30$$

As the variation in Ψ' is complex and arbitrary,

$$< \delta\Psi' | H^* - \lambda + \gamma g \left(\mu_A^0\right)^2 | \Psi' > = 0$$

and

$$< \Psi' | H^* - \lambda + \gamma g \left(\mu_A^0\right)^2 | \delta\Psi' > = 0$$

Identifying λ with E_s, the energy of the solute in the gas phase, and $\gamma = 1/2$,

$$H^* | \Psi' > = \left(E_s - \frac{1}{2} g \left[\mu_A^0\right]^2 \right) | \Psi' > \qquad 2.31$$

Thus, if the Hamiltonian of the solute is defined as in equation (2.28), the energy E of the solute in the presence of the continuum solvent is given by

$$E = E_s - \frac{\left(\mu_A^0\right)^2}{a^3} \left\{ 2 \left(\frac{\epsilon - 1}{\epsilon + 2} \right) - \left(\frac{n^2 - 1}{n^2 + 2} \right) \right\} \qquad 2.32$$

Clearly, the solvent induced energy change in the solute is due to the reaction fields, one arising from the interaction of the permanent dipoles and the other due to the coupling of the solute dipole with the polarizability of the solvent. Therefore, the corrections to the gas phase energy of the solute include corrections through first order and part of the second order terms.

Defining the Hamiltonian as in equation (2.28), the method presented above was incorporated into the INDO formulation of Ridley and Zerner (12) and Bacon and Zerner (13). The ground state wavefunction $| \Psi' >$ for the solute, having 2N valence electrons, in the solvent was described by a single determinant in the molecular spin orbitals ψ_i { i = 1, 2, ..., N }. The excited states were determined by single excitations within this determinant. The Fock operator F' for the solvated molecule was defined by

$$F' = F_0 - \frac{1}{2} g < \hat{\mu} > .\hat{\mu}$$

where g has been defined in equation (2.27) and F_0 is the Fock operator for the solute in the gas phase within the INDO approximation. Comparing the terms in equation (2.32) with equation (2.25), the energy of the excited state under consideration has to be corrected by the term τ where

$$\tau = \{\mu_A^0 . \mu_A^e - (\mu_A^e)^2\} \frac{1}{a^3} \left(\frac{n^2 - 1}{n^2 + 2} \right) \qquad 2.33$$

To evaluate this correction, the only additional quantity required is the dipole moment of the excited state of interest. For the numerical calculations, the dielectric constant and refractive index were obtained from experiment, and the

dipole moments of the ground and excited states of the solute calculated using the INDO method. The only other variable that has to be determined is the cavity radius 'a', and the methods used are outlined in the following section.

2.5 Determination of the Cavity Radius ' a '

In their studies on the dissociation of HF in water using the reaction field method, Karelson Katritzky, and Zerner (20) calculated the cavity radius from the molar refraction according to

$$\frac{4}{3}\pi a^3 = \frac{M}{\rho N_A}\left(\frac{n^2-1}{n^2+2}\right) \qquad 2.34$$

where n and N_A are the refractive index of the solute and Avagadro's number. M and ρ are the molecular mass and the mass density. However, this method suffers from a major drawback in that solutes whose refractive indices are close to unity are calculated to have negligible radii. A good example is acetylene; the refractive index is 1.00051 and the radius, according to equation (2.34), is 0.178A.

Another method to evaluate radii is from effective volumes of organic substituent groups proposed by Bondi (21). The values for 'a' are realistic, but when used in the evaluation of the spectral shifts as outlined in the previous section, gave results in poor agreement with experiment.

Calculation of the cavity radius from the mass density is another possibility. The radius 'a' is calculated according to

$$\frac{4}{3}\pi a^3 = \frac{M}{\rho} \qquad 2.35$$

The spectral shifts calculated using this method are in much better agreement with experiment than those obtained from Bondi's radii.

Fitting a scaled cavity radius obtained from equation (2.35) to the calculated spectral shifts indicated that a radius that is 1.5 times that calculated from the mass density gave the best fit for ortho-nitroaniline. It was therefore decided to use this technique to obtain the cavity radius for the calculation of the solvent induced spectral shifts. The values used for the cavity radius are given in Table 2.1.

TABLE 2.1 Cavity radius (A) for the solute molecules.

SOLUTE	RADIUS (A)
o-nitroaniline	5.08
m-nitroaniline	5.54
p-nitroaniline	5.51
p-nitrophenol	5.50
pyridine	4.76
phenol	5.01

2.6 Results of Calculations and Disussion

Using the method outlined in sections 2.4 and 2.5, the shifts in the electronic spectra of a series of molecules in various solvents were determined. The results are tabulated below along with the values for the cavity radii (in A) used in the calculations. The geometries of the solute molecules were obtained from X-ray

data, and the dielectric constant and refractive index were taken from standard tables (22) and are listed in Table 2.2.

TABLE 2.2 Dielectric constant (ϵ) and Refractive index (n) for the solvents.

SOLVENT	ϵ	n
n-hexane	1.890	1.3751
n-pentane	1.844	1.3575
n-octane	1.948	1.3974
cyclohexane	2.023	1.4266
CS_2	2.641	1.6319
ethanol	24.3	1.3661
methanol	32.63	1.3288
water	78.0	1.33

The active space for the singles only configuration interaction scheme was confined to the five highest occupied and five lowest unoccupied molecular orbitals. A calculation using a full singles only space for pyridine in hexane and in ethanol gave a spectral shift improved by only ten wavenumbers. It was thus decided to use the previously defined active space of ten molecular orbitals in all the calculations as the results obtained from a full singles only space did not justify the time and effort required for their evaluation.

The origins of the calculated and experimental shifts for all the results given in this chapter are the gas phase transition values obtained using the INDO scheme

and experiment respectively. These values are given in Table 2.3. A negative sign for the solvent induced shift indicates a red shift with respect to the corresponding origin.

TABLE 2.3 Gas phase spectra of the solute molecules.

SOLUTE	CALCULATED TRANSITION (cm^{-1})	EXPERIMENTAL TRANSITION (cm^{-1})
o - nitroaniline	27,400	28,200 (ref 23)
m - nitroaniline	28,710	30,900 (ref 23)
p -nitroaniline	31,699	34,480 (ref 23)
p - nitrophenol	33,302	37,310 (ref 23)
pyridine	38,194	38,350 (ref 24)
phenol	36,950	36,352 (ref 25)

TABLE 2.4 Shifts in the $\pi \rightarrow \pi^*$ spectrum of o – nitroaniline.

SOLVENT	CALCULATED SHIFT (cm^{-1})	EXPERIMENTAL SHIFT (cm^{-1}) (ref 23)
ethanol	-2543	-3321
n - hexane	-2040	-1590
n - pentane	-1955	-1500
cyclohexane	-2282	-1700
n - octane	-2148	-1690
CS_2	-3217	-2680

TABLE 2.5 Solvent shifts in the $\pi \rightarrow \pi^*$ spectrum of m – nitroaniline.

SOLVENT	CALCULATED SHIFT (cm^{-1})	EXPERIMENTAL SHIFT (cm^{-1}) (ref 23)
n - hexane	-2554	-1920
n - pentane	-2438	-1830
cyclohexane	-2867	-2100
CS_2	-4144	-2970

TABLE 2.6 Shifts in the $\pi \rightarrow \pi^*$ spectrum of p – nitroaniline.

SOLVENT	CALCULTED SHIFT (cm^{-1})	EXPERIMENTAL SHIFT (cm^{-1}) (ref 23)
n - hexane	-3688	-3130
n - pentane	-3529	-2810
cyclohexane	-4136	-3410
CS_2	-5914	-5280

TABLE 2.7 Shifts in the $\pi \rightarrow \pi^*$ spectrum of p – nitrophenol.

SOLVENT	CALCULATED SHIFT (cm^{-1})	EXPERIMENTAL SHIFT (cm^{-1}) (ref 23)
cyclohexane	-2799	-2340
n - hexane	-2482	-2100
n - heptane	-2562	-2340

The geometries used for the nitroanilines and p-nitrophenol were obtained from references (26) and (27) respectively.

In each of the four cases presented above, the calculated shifts parallel the experimental values for each solute in the various solvents. With the exception of o-nitroaniline in ethanol, the calculated shifts are overestimated by approximately 300 to 1000 wavenumbers towards the red side of the electromagnetic spectrum. This agreement with experiment is considered to be excellent within the approximations of the model.

The calculated red shift for the solvation of o-nitroaniline in ethyl alcohol is lower than the experimental value. In order to rationalize this observation, the basic assumptions of the model have to be reviewed. The reaction field equations were derived based on the theory of weak interactions between the solute and the solvent. Furthermore, the solvent was considered to be isotropic. These assumptions hold more closely when the solvent is nonpolar, in which case the intermolecular interactions are small and the specific arrangement of the solvent

TABLE 2.8 Shifts in the $\pi \rightarrow \pi^*$ spectrum of pyridine.

SOLVENT	CALCULATED SHIFT (cm^{-1})	EXPERIMENTAL SHIFT (cm^{-1})
water	290	713 (ref 28)
ethanol	347	560 (ref 29)
n-hexane	27	1491 (ref 30)
cyclohexane	32	1491 (ref 30)
methanol	313	1176 (ref 30)

TABLE 2.9 Shifts in the $\pi \rightarrow \pi^*$ spectrum of phenol.

SOLVENT	CALCULATED SHIFT (cm^{-1})	EXPERIMENTAL SHIFT (cm^{-1})
ethanol	69	279 (ref 31)
methanol	75	278 (ref 32)
water	84	685 (ref 33)
cyclohexane	7	413 (ref 33)
hexane	6	548 (ref 34)

X-ray geometries for pyridine and phenol were obtained from references (35) and (36) respectively.

The influence of the solvent on the ground and excited states of the solute molecule is responsible for the observed spectral shift. If the ground state of the

solute is polar, it will be stabilised by a polar solvent. As the time interval of the electronic transition is small, the solvent cage does not have sufficient time to rearrange itself to accommodate the changed dipole of the solute excited state. If the dipole moment or the largest Cartesian component of the dipole is larger and parallel to the corresponding property of the molecule in the ground state, the excited state solute will be stabilized to a greater extent than the ground state, resulting in a red shift in the spectra. Clearly, a nonpolar solvent in the above case will yield a blue shift.

In cases where the excited state has a lower dipole than the ground state, the solvent will not stabilize the excited state as much as the ground state, resulting in a blue shift in the electronic spectrum. If the solvent were nonpolar, the direction of the shift will be in the opposite direction, thus causing a red shift in this case. The situations discussed in this and the preceding paragraph apply to $\pi \rightarrow \pi^*$ transitions.

The n-orbital is responsible for the hydrogen bond formation between a polar molecule and a polar solvent. During an $n \rightarrow \pi^*$ transition, an n-electron is removed from the non-bonding orbital and promoted to the π^* orbital thereby destroying the hydrogen bond. Thus the excited energy is raised by an amount equal to the strength of the broken bond causing a blue shift.

The spectra studied for both pyridine and phenol are of the $\pi \rightarrow \pi^*$ type, and according to the discussion presented in the preceding paragraphs should have red shifts in polar solvents and blue shifts in nonpolar environments. Both molecules

are predicted to have hypsochromic shifts in all the solvents studied in agreement with experiment.

The polar molecules, water, ethanol and methanol have acidic hydrogens which can protonate the nitrogen atom in pyridine. Thus, the solute that is being investigated experimentally is no longer pyridine, but the pyridinium ion which is now stabilized by strong hydrogen bonding with the solvent molecules resulting in a blue shift in the $\pi \rightarrow \pi^*$ spectrum. The blue shift is predicted to increase with increasing acidity of the solvent, an effect that has been observed experimentally(30).

Recent multiphoton resonance spectral studies on the stepwise hydration of phenol (35) show that the lowest $\pi \rightarrow \pi^*$ spectrum of phenol / $(H_2O)_1$ gives a red shift indicating that the phenol is behaving as an acid. Further hydration shows a continuous blue shift in the spectrum of the solute due to the stabilization of the phenolic anion by the solvent molecules which are capable of hydrogen bonding, an effect very similar to the case of pyridine.

Thus, the general guidelines for the prediction of the spectral shifts in polar and nonpolar solvents presented earlier in this section are helpful only if the solvent does not change the nature of the solute.

2.7 Conclusions

The continuum model works very well for solutes in nonpolar solvents, provided a judicious choice is made for the cavity radius. In the case of polar solvents, the predictive power of the method is not very useful, in that the value

calculated for the shift is not in very good agreement with experiment. However, the direction of the shift is always reproduced correctly.

Three immediate improvements to the method, as outlined in this chapter are clear. The first would be to determine the cavity radius using a more reasonable algorithm as the spectral shift is strongly dependent on this parameter. If the value of this radius is too large, the solvent effect is underestimated, sometimes resulting in shifts that are nearly zero. A cavity which is too small overestimates the shift giving results that are physically unrealistic. Examples of such cases are discussed in Chapter 4 where a suitable choice for the radius has to be made in order to include previously determined solvent shells explicitly. Furthermore, the same value for the radius has been used for the ground and excited states. The excited state, especially when the solvent is polar, would be expected to have a larger radius as the solvent would stabilize the more diffuse charge density and hence the larger dipole. It may thus be necessary to use different values for the cavity radii when treating the ground and excited states.

In all the applications presented in this chapter, the solute molecules have permanent dipoles. The reaction field theory, as presented here, is applicable only to such molecules and this restricts any investigations on nonpolar molecules like benzene. However, such molecules can be studied using this formulation if the two second order terms, namely $E_1^{(2)}$ and the dipersion energy $E_3^{(2)}$ ignored here are explicitly considered. The term $E_1^{(2)}$, which is the energy contribution due to the polarization of the solute by the solvent, will be the leading term in

the multipolar expansion of the interaction energy for nonpolar systems and the dispersion energy term will also be appreciable. A second improvement would then involve extension of the method to include these two terms.

The third improvement is to explicitly consider the structure of the solvent molecules, particularly those in the vicinity of the solute molecule. After constructing these solvent shells, the solvated solute complex can then be immersed in the continuum solvent, the radius of the cavity for the complex having been suitably determined. The solvation shells would introduce solvent anisotropy, an effect overlooked by the continuum fluid model. A method for the construction of such solvation shells is presented in the next chapter.

CHAPTER 3
SEARCH FOR THE GLOBAL MINIMUM ON A POTENTIAL ENERGY SURFACE

3.1 Introduction

To obtain the most stable structure of solvent molecules around a solute, it is necessary to find the global minimum on the potential energy surface (PES) that describes the solute-solvent interactions. This search can be accomplished in two ways, namely

1. Sequential search — gradient based methods, and
2. Random search techniques.

The sequential search algorithms require the evaluation of the gradients f_i at points r_i on the surface (38) which are generated from an arbitrarily chosen starting point r_0 according to the equation

$$\vec{r}_{i+1} = \vec{r}_i - \alpha f_i H^{-1} \qquad 3.1$$

where i = 0, 1, 2, . . . , N

α is the step size on the surface

H is the second derivative of the energy matrix and

N is the number of steps allowed in the search.

For a simple PES with one or very few minima which are sparsely distributed, the gradient search is efficient in locating these minima. However, for systems with many degrees of freedom, like those found in problems dealing with solvation, the gradient method fails. This is because the search can be trapped in any one of the local minima and the algorithm does not have a mechanism by which it can move out of such minima.

Furthermore, r_0 defines the point on the the PES at which the search is initiated. The success of the algorithm depends on the choice of this point, and, in the case of surfaces with multiple minima, the scheme is efficient only if r_0 is in the neighborhood of the global minimum. If this condition is not satisfied, the local minimum closest to the choice of r_0 will be calculated. However, the advantage in using gradient type methods is that they are computationally less time consuming.

Random search techniques, on the other hand, do not have these disadvantages. The potential energy surface is scanned at random, the new point sampled being a function of a predetermined step size of the various degrees of freedom. The method of Simulated Annealing (39,40) as adapted by Donnelly (41) is an example of a random search technique which is applicable to problems in intra– and intermolecular interactions. As the systems studied in this thesis deal with the latter category, the outline of the method presented here will emphasize only this aspect of the algorithm.

3.2 The Simulated Annealing Method

A very successful method by which the equilibrium properties of systems can be evaluated is the Metropolis Monte Carlo algorithm (42). Thermodynamic observables are a statistical average of the property measured, and this average is over an order of the Avagadro's number in the constituent particles. Computationally, such calculations are impossible and it is therefore necessary to simulate the bulk properties from a small, but physically meaningful number of particles. The choice of this number, say N, should be so as to minimize the fluctuations in the calculated value of the property.

The N particles are assumed to interact with each other and this interaction is described by an interparticle potential energy function U(r,Ω). The variables r and Ω represent, respectively, the distance separating the particles and any other coordinates such as the angles of orientation that the potential energy might depend on. The interparticle interaction energy ΔE is then given by

$$\Delta E = \sum_{i,j,\ldots,N,\, r_i,r_j,\ldots,N,\, \Omega_i,\Omega_j,\ldots,N} U(r_i, r_j, \Omega_i, \Omega_j, \ldots N) \qquad 3.2$$

In the Monte Carlo method, the N particles are placed in a cube whose volume V has been chosen to reproduce experimental data on the mass density of the system to be simulated. The initial configuration of the particles is arbitrary and this flexibility is one of the tremendous advantages of this method. Using equation (3.2), ΔE for the initial arrangement is evaluated.

A particle i at position $r_i = (x_i, y_i, z_i)$ is chosen at random and moved according to

$$x_i' = x_i + dn_1$$

$$y_i' = y_i + dn_2$$

$$z_i' = z_i + dn_3 \qquad 3.3$$

.....

$$\Omega_i' = \Omega_i' + fn_k$$

where d and f are previously chosen step sizes for the changes in the displacement r and Ω variables. The set $\{n_i\}$ i=1,2, ..., are random numbers in the interval [-1,1].

If the move takes the particle out of the cube, the particle is brought back into the volume V from the direction which is the mirror image of the displacement that took the particle out of the cube. This requirement reduces the surface effects and maintains the mass density at its predetermined value.

The interaction energy in the new configuration $\Delta E'$ is now calculated using equation (3.2). If $\Delta E'$ is less than the value calculated for the previous configuration, the new arrangement of the particles is accepted and the process of choosing a particle and moving it to a newer configuration repeated. In cases where $\Delta E'$ is greater than the previous value for the interaction energy, a probability p, given by

$$p = exp\left[-\left(\Delta E' - \Delta E\right)/kT\right] \qquad 3.4$$

is calculated. k and T refer to the Boltzmann constant and the thermodynamic temperature respectively. If p is greater than a random number belonging to the interval [0,1], the move of the particle to the new configuration is accepted and

the algorithm proceeds as descibed above. On the other hand, if p is less than the random number, the new configuration is rejected and the particle brought back to its position prior to the move. A particle is again chosen, moved according to equation (3.3), and the method repeated until no further configurations are accepted. When this criterion is satisfied, the system is said to have reached its equilibrium configuration.

The efficiency with which this minimum is reached according to the Metropolis algorithm will depend on the number of moves allowed for the displacement of the particles. The equilibrium configuration of the particles will be determined more accurately if the number of moves allowed is very large in the random walk process.

The simulated annealing method makes use of the Monte Carlo algorithm outlined above. The main difference is that the probability p is now calculated according to

$$p = exp\left[-\left(\Delta E' - \Delta E\right)/T^*\right] \qquad 3.5$$

where T^* is now a parameter which has the same units as energy. For a given value of T^* the potential energy surface is scanned in a finite number of moves using the random walk process described. T^* is then varied using an annealing factor β as

$$T^*_{i+1} = \beta T^*_i, \qquad 0 < \beta < 1 \qquad 3.6$$

The index i refers to the number of annealing steps allowed. The entire search process is repeated with the new value of T^*. As T^* decreases, areas of the the

surface closer to the minimum are scanned and if any minima had been missed by the search using the previous value of T^*, the algorithm can now lock itself onto a lower minimum. As the number of cycles allowed for the annealing step increases, the search for the global minimum becomes more efficient as minima of lower energy can be searched. This flexibility in being able to anneal the PES is one of the assets of the simulated annealing method.

Unlike gradient search techniques in which the displacement or steps are on the potential surface, the random displacements in annealing enable the search to tunnel out of any local minima in which the algorithm could have got trapped. The decrease in T^*, which allows narrower areas of the surface to be searched coupled with the tunneling advantages assures the evaluation of the global minimum provided the algorithm has been allowed a large enough number of random moves for each value of T^*.

3.3 Choice of Potential Energy Function

In order to apply the annealing method described in the previous section, the interaction energy has to be evaluated. This requires a prudent choice of $U(r,\Omega)$. A quantum mechanical calculation is impractical as the energy has to be evaluated for changes in every intersystem coordinate. The energy of interaction ΔE can be expressed as a series according to (5)

$$\Delta E = \sum_{i,j} U(r_i, r_j, \Omega_i, \Omega_j) + \sum_{i,j,k} U(r_i, r_j, r_k, \Omega_i, \Omega_j, \Omega_k) + \ldots \quad 3.7$$

where $U(r_1, \ldots, r_m, \Omega_1, \ldots, \Omega_m)$ is the m-body contribution to the interaction energy. The various terms in the above equation refer to summations over the atomic centers of the constituent systems.

Application of equation (3.7) to a problem that deals with molecular solvation on a macroscopic scale is not computationally feasible. The main reason is the number of terms that have to be evaluated. Even if a simulation of the macroscopic system is executed with N molecules, this problem still remains as each m-body term will have N^m calculations. This number is astronomical even for small N for which the series expansion of ΔE has higher order terms in the interaction. As such, it is necessary to truncate the series at a reasonable order in the interaction which incorporates the physics of interest. Expressing ΔE as a sum of interactions over pairs of atomic centers is a method commonly used.

If the distance R_{AB} separating the systems A and B is much larger than the dimensions of the interacting species itself, the energy of interaction can be evaluated using the theory of weak interactions. Within this theory, ΔE is expressed as a multipolar expansion in the inverse powers of R_{AB} as (5)

$$\Delta E = \sum_{n=1}^{\infty} C_n / R_{AB}^n \qquad 3.8$$

The coefficients C_n contain the physics of the interaction. For example when

n=1, C_1 is given by

$$C_1 = q_A q_B \qquad 3.9$$

which is the coefficient of the coulombic term. q_A and q_B are the charges on systems A and B respectively. The higher order coefficients contain dipole moments, polarisabilities and higher order moments of the interacting species.

If A and B are molecular systems composed of a and b atomic centers respectively, the pairwise interaction approximation expresses ΔE as

$$\Delta E = \sum_{n=1}^{\infty} \sum_{i=1}^{a} \sum_{j=1}^{b} C_n / R_{ij}^n \qquad 3.10$$

Clearly, the infinite sum in the above equation is a restriction to the evaluation of the interaction energy. It is thus necessary to truncate equation (3.10) to a finite number of terms. Many successful applications using the series of approximations outlined above are available in the literature (43,44).

The coefficients C_n for truncated pairwise potentials can be obtained in many ways. One method is to use the electronic moments obtained from experiment together with classical or quantum mechanical charge densities. Such a method suffers from a serious drawback in that the static moments used do not always simulate the interactions accurately and the experimental values contain many body effects which have been neglected in

the pairwise approximation. For example, the description of the interaction of a positive ion with a neutral molecule should be able to account for the change in the polarizabilities of the interacting systems due to charge transfer effects, a phenomenon that is neglected when static moments are used.

Another method is to fit a multipolar expansion to thermodynamic data for the systems studied. A good example of such a parameterisation is the potential energy function determined for water by Jorgensen et al (45). The Bernal and Fowler model (46) is used to describe the water molecule, according to which a molecule of water is comprised of four coplanar points, namely the three atoms and a pseudocenter M on the bisector of the HOH angle. This point is at a distance of 0.15A from the oxygen atom.

The interaction energy ΔE is given by

$$\Delta E = \sum_{i<j} q_i q_j / R_{ij} - \sum_{i<j} A_{ij}/R_{ij}^6 + \sum_{i<j} B_{ij}/R_{ij}^{12} \qquad 3.11$$

The summations are over the centers on the water molecule, q_i is the quantum mechanical charge density on center i and A_{ij} and B_{ij} are coefficients determined as described below. Using equation (3.11), a Monte Carlo simulation of the thermodynamic properties of water like the specific heat and isothermal compressibility is carried out. A_{ij} and B_{ij} are varied to reproduce these quantities as closely as possible to experimental data. The values obtained for the parameters used in equation (3.11) are given in Table 3.1.

TABLE 3.1 Parameters for equation (3.11)

PARAMETER	VALUE
r(OH A)	0.9572
r (OM A)	0.15
Angle HOH, deg	104.52
A (kcal A^6/mol)	610.0
B x 10^{-3},kcal A^{12}/mol	600.0
q (O)	0.0
q (H)	0.52
q (M)	-1.04

The use of such potential energy functions is costly as simulations are required for every system that is to be studied. The transferability of these parameters for the study of mixed systems, that is, systems with more than one chemical species, is questionable as the specificities of the interactions in mixed systems have to be considered. Furthermore, a set of parameters for each pair of interacting atoms is required to define the potential for a variety of systems.

A very practical approach to parameterising a potential energy function that can be applied to a variety of systems was presented by Fraga (47). Instead of determining parameters for every pairwise interaction, the atoms in the interacting systems are assigned to classes based on the average one center contribution to the Hartree-Fock energy called the Molecular Orbital Valency State (MOVS) (48).

The energy of interaction ΔE is calculated as

$$\Delta E = \sum_{a,b} \{ q_a q_b / R_{ab} - \frac{1}{2} \left[f_a \alpha_a q_b^2 + f_b \alpha_b q_a^2 \right] / R_{ab}^4$$

$$- \frac{3}{2} \left(f_a f_b \alpha_a \alpha_b / \left[(f_a \alpha_a / n_a)^{1/2} + (f_b \alpha_b / n_b)^{1/2} \right] R_{ab}^6 \right) \qquad 3.12$$

$$+ g_a g_b / R_{ab}^{12} \}$$

where the summation indices (a,b) are now over the classes to which the atoms belong. q_x, α_x, n_x, f_x and g_x (x=a,b) are respectively, the electronic charge, the static polarisability, the effective number of electrons and parameters for class x. q_x is obtained from quantum mechanical calculations (49) and the polarisability is calculated by extrapolating Hartree-Fock data for the atom and its ions (50) that have been assigned to class x. n_x, the effective charge is given by

$$n_x = Z_x - q_x \qquad 3.13$$

where Z_x is the atomic number of the atom that has been assigned to class x. f_x and g_x are obtained by fitting equation (3.12) to ab-initio results of Clementi et al (49) for the interaction of twenty six amino acids with water. Table 3.2 gives the parameters for the atoms (47) and ions (51) and a description of their environments.

TABLE 3.2 Parameters for Atoms and Ions.

ATOM	CLASS	q	$\alpha(A^3)$	f	g ($kcal^{1/2}$ A^6 $mol^{-1/2}$)	ENVIRON-MENT
H	23	0.060	0.42	.85	69.3	- SH
	2	0.204	0.36	0.1	162	- CH, CH2
	3	0.205	0.36	0.1	22.3	- CH3
	16	0.253	0.34	0.1	131	- CH, AROMATIC C
	1	0.266	0.33	0.35	1.28	- NH2
	4	0.404	0.29	0.95	5.53	- COOH
C	6	-0.608	3.60	0.10	536	- CH3
	21	-0.503	3.20	0.10	21.2	- CH2, ALPHA TO S
	7	-0.383	2.75	0.10	508	- CH2
	17	-0.218	2.20	0.10	948	AROMATIC C

TABLE 3.2 (continued)

ATOM	CLASS	q	$\alpha(A^3)$	f	g ($kcals^{1/2}$ A^6 $mol^{-1/2}$)	ENVIRON-MENT
C	8	-0.135	2.00	0.10	362	- CH
	28	-0.090	1.90	0.10	72	AROMATIC C, ALPHA TO -CH3
	14	-0.078	1.90	0.10	234	AROMATIC C, ALPHA TO N
	19	-0.032	1.80	0.10	13.4	AROMATIC C, GEMINAL TO C
	18	0.008	1.70	0.10	186	AROMATIC C, PHENOLIC.

TABLE 3.2 (continued)

ATOM	CLASS	q	$\alpha(A^3)$	f	g ($kcal^{1/2}$ A^6 $mol^{-1/2}$)	ENVIRON-MENT
C	24	0.310	1.30	2.60	982	ADJACENT TO NH_2
	26	0.423	1.20	0.10	385	AROMATIC, CO
	5	0.511	1.10	0.10	667	CARBO-XYLIC
N	13	-0.630	2.35	0.10	1111	AMIDE
	11	-0.554	2.10	0.15	245	AMINO
	15	-0.473	1.90	0.95	998	AROMATIC, WITH H
	12	-0.317	1.50	0.10	362	AROMATIC, WITHOUT H
S	22	0.123	3.15	0.35	1035	SH

TABLE 3.2 (continued)

ATOM	CLASS	q	$\alpha(A^3)$	f	g ($kcal^{1/2}$ A^6 $mol^{-1/2}$)	ENVIRON-MENT
O	9	-0.539	1.45	0.21	555	OH, in COOH
	10	-0.409	1.25	0.10	476	CO, IN COOH
	27	-0.380	1.20	0.80	268	CO, ATTACHED TO RING
O	30	-0.622	1.65	0.95	548	H_2O
H	29	0.311	0.32	0.90	547	H_2O
Na^+	32	+1.00	0.15	5.1	563	
K^+	33	+1.00	0.95	1.00	1415	

Both potential functions mentioned above were used to evaluate the interaction energy of simple systems. The water dimer was the first example studied using the simulated annealing method. The initial orientation for the system is given in Figure 3.1. The geometry used for the water molecule was obtained from reference (52) and the results obtained are listed in Table 3.3. θ is the angle made by the OH bond of the second molecule with the bisector of the HOH angle of the first molecule.

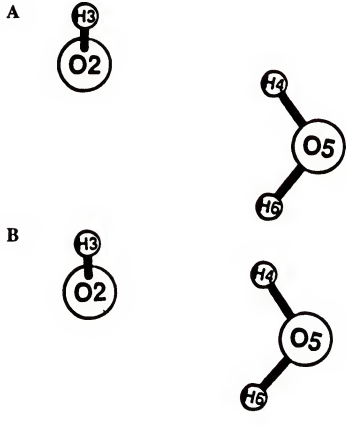

Figure 3.1 Initial (A) and final geometries (B) for the water dimer.

3.4 Results and Discussion of the Simulated Annealing Method

The starting configuration for the water dimer (Figure 3.1) used in the previous section is one that is very close to the equilibrium configuration. The potential of the annealing method lies in the fact that the results are independent of the initial arrangement of the molecules. In order to illustrate this aspect of the algorithm, the calculation on the water dimer was repeated with the two molecules arranged as shown in Figure 3.2.

Figure 3.2 Initial random geometry for the water dimer.

The configuration shown above has a very high energy as the lone pairs on the oxygen atoms repel each other. A gradient search technique fails to give a minimum even after many hours of computation as the two molecules repel

TABLE 3.3. Calculated and experimental results for the water dimer using the Jorgensen (9) and Fraga (11) potentials.

PROPERTY	EXPERIMENT (52-54)	JORGENSEN POTENTIAL	FRAGA POTENTIAL
r O-H (A)	0.9572		
HOH	104.52		
ΔE (kcals/mole)	-5.44	-6.28	-5.07
θ deg	50 - 70	73.9	66.2
r O_1O_2	2.98	2.91	2.89

The interaction energy ΔE we obtained using the first potential function is lower than the value of – 6.24 kcals/mole reported by Jorgensen et al (45) from their Monte Carlo simulation, indicating that the minimum they had evaluated with their potential is not the global minimum for the system. Further, the agreement with experiment for the other parameters is not nearly as good as that obtained using the Fraga potential.

One area of study presented in this dissertation is the interaction of molecules with a wide range of solvent systems. It is therefore important to have one potential energy function which has been consistently parameterised and applicable to as many systems as possible. The comparison of results obtained for different systems from simulations that have been parameterised by various means loses meaning in their interpretation. Taking these points into consideration, it was decided to use the Fraga potential in all the simulations to be presented in this thesis. The results of these simulations are presented in the following section.

each other very slowly. The simulated annealing method is very successful as the results given below illustrate.

TABLE 3.4 Results for the water dimer

PROPERTY	GEOMETRY (FIGURE 3.1)	GEOMETRY (FIGURE 3.2)	EXPERIMENT (ref 52-54)
ΔE (kcals /mole)	-5.07	-5.07	-5.44
r O_1O_2 (A)	2.89	2.89	2.98
θ deg	66	67	50 - 70

The calculated properties for the water dimer shown in coloumns 2 and 3 of table 3.4 show that the results are independent of the starting configuration and in excellent agreement with experiment. Thus, the initial configuration of the systems to be simulated need not be chosen beforehand to be close to the equilibrium arrangement of the molecules — a bias usually introduced in gradient search methods, (but not for this case).

The water trimer was studied next. The global minimum evaluated corresponds to a cyclic structure in which the three oxygen atoms form an isoceles triangle. Infra–red studies (55) show the trimer to be cyclic with the oxygen atoms at the vertices of an equilateral triangle. A possible reason for the discrepancy between the calculated and experimental results lies in the manner in which the interaction energy is evaluated. The evaluation of the interaction energy as a sum of pair-wise terms neglects three body and higher effects, contributions which

are present in experimental studies. Although these terms may be comparatively small, they could accumulate to favour a different structure from that obtained from a pair-wise expansion. Calculations on the water tetramer gives a cyclic structure as the most stable configuration in agreement with other calculations reported (56–58).

Another example of a system stabilised by hydrogen bonding is the acetic acid dimer. A series of minima were obtained and these values are given in Table 3.5. The global minimum corresponds to an interaction energy of – 9.46 kcals/mole and the structure of the dimer is given in Figure 3.3.

At the global minimum, the carboxylic groups in the monomers are coplanar facilitating maximum hydrogen bonding between the carbonyl oxygen of one molecule and the hydrogen atom of the —OH group of the other. In each of the structures that correspond to the local minima, the two —COOH groups are not coplanar resulting in structures of higher energies due to reduced hydrogen bonding.

TABLE 3.5 Minima for the acetic acid dimer

MINIMUM	ΔE (kcals/mole)
Local	-6.87
Local	-7.81
Local	-8.13
Local	-8.29
Local	-9.22
Global	-9.46

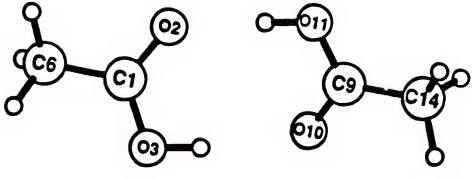

Figure 3.3 Orientation of the monomers of acetic acid at their global minimum.

In their studies on the benzene-water system, Karlstrom et al (59) report two minima — the global minimum being 1.09 kcals/mole below the local minimum. The annealing method gives very similar results which are tabulated below. The two sets of results in Table 3.6 are not directly comparable as the potential energy functions used in their evaluation are different — the emphasis is on the trends and similarities between them.

TABLE 3.6 Results for the benzene-water system

PROPERTY	SIMULATED ANNEALING	KARLSTROM et al (ref 59)
ΔE (kcals/mole) (local minimum)	-1.77	-1.90
ΔE (kcals/mole) (global minimum)	-2.66	-2.99
θ deg	0.09	0.1
R (A)	4.75	3.5

The global minimum for this system is shown in Figure 3.4. Both methods give the same orientation for the subsystems, although the intermolecular distance R, measured from the oxygen atom to the center of the benzene ring, is different.

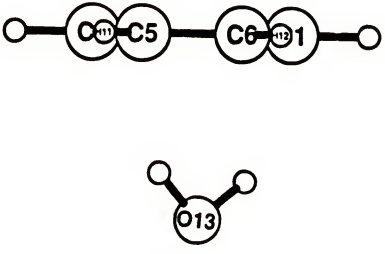

Figure 3.4 Global minimum for the benzene — water system.

Clusters of molecules can be formed by the stepwise addition of monomers. The simulated annealing method was applied to the formation of such clusters or microdroplets. The global minimum for the stepwise formation of each cluster was calculated and at each step in the buildup procedure, all the molecules were allowed to move according to the algorithm.

Based on the solvophobic theory of Sinanoglu (60), it is possible to determine the number of molecules in a microdroplet, which is defined as the smallest possible cluster of the constituent molecules that approaches bulk behaviour. Using the experimental values for the surface tension and isothermal compressibility, the number of molecules in a cluster have been calculated. For water, a cluster of fifteen molecules was found to have 95% of the bulk surface tension, while for benzene six molecules satisfied this criterion.

The water and benzene systems were studied using the annealing method. The interaction energy per molecule in the cluster, ΔE_1, was evaluated for droplets of increasing size. The results for benzene are tabulated below and the structure for the dimer is shown in Figure 3.5. The dimerisation energy for benzene was calculated to be 1.50 kcals/mole, well within the experimental range of 1.15 to 2.07 kcals/mole (61).

TABLE 3.7 Simulation of the microdroplet of benzene

NUMBER OF MOLECULES N	ΔE_1 (kcals/mole)
2	-0.75
3	-1.08
4	-1.33
5	-1.55
6	-1.43
.	.
10	-1.44

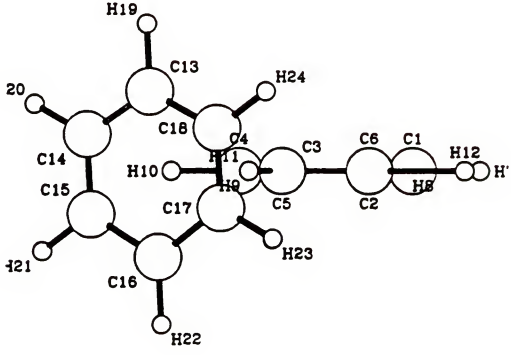

Figure 3.5 Structure of the benzene dimer at its global minimum.

The T-shaped structure obtained for the dimer of benzene is in agreement with experimental results (61) and quantum chemical studies (62,63). A plot of ΔE_1 versus the number of molecules N is shown in Figure 3.6. From the graph, the number of molecules of benzene that can form a cluster with no appreciable further stabilisation is five and the structure of this pentamer is shown in Figure 3.7

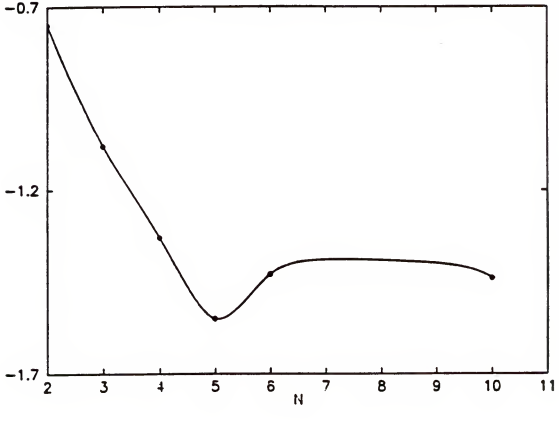

Figure 3.6 Interaction energy per molecule versus N for $(benzene)_N$.

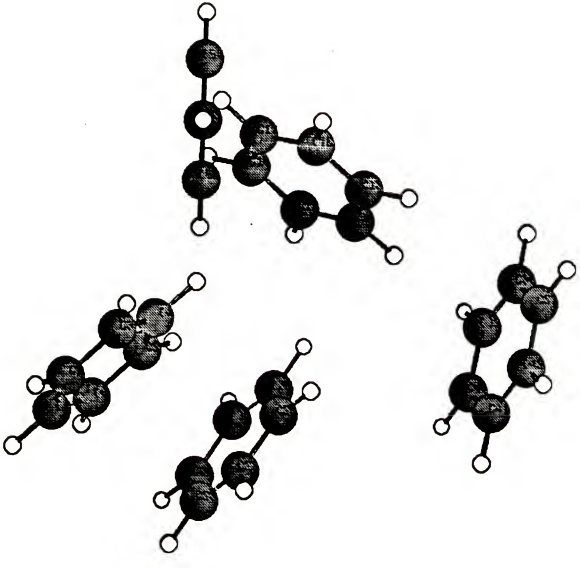

Figure 3.7 Structure of the benzene pentamer.

The curve shown if Figure 3.6 goes up for the hexamer and larger clusters. The difference in the energy between the minimum for the pentamer and that for the larger clusters is only 0.11 kcals/mole. This is attributed to be an artifact introduced by the potential energy function. The structure of the pentamer (Figure 3.7) shows the molecules to be arranged perpendicular to each other, corresponding to a ligand-like structure. in agreement with other theoretical calculations (62).

A similar treatment of the water cluster yielded the results shown in Table 3.8 and the plot of the interaction energy per water molecule versus N, the number of molecules, is given in Figure 3.8

From this figure, the stabilisation of a cluster of water molecules shows no further gain beyond N = 16. The microdroplet of water is thus found to have sixteen water molecules, in excellent agreement with the results of Sinanoglu (60) who reports a value of 15. The structure of this droplet is shown in Figure 3.9. The stabilisation observed at N = 5 corresponds to the water pentamer. Recent theoretical studies (64) show that the first solvation shell of a water molecule has four other molecules arranged tetrahedrally around the central molecule. The structure of the pentamer calculated by the annealing method is shown in Figure 3.10.

TABLE 3.8 Results of the simulation of the water cluster

NUMBER OF MOLECULES N	ΔE_1 (kcals/mole)
2	-2.25
3	-4.19
4	-5.26
5	-5.31
6	-5.62
8	-6.47
10	-6.90
12	-7.25
14	-7.38
16	-8.01
18	-7.97
20	-7.35
.	.
25	-7.30

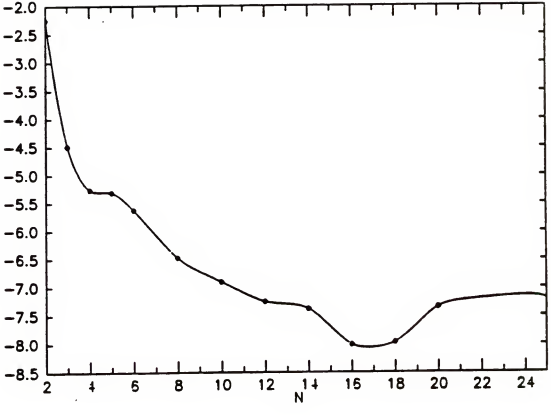

Figure 3.8 Interaction energy per molecule versus N for $(H_2O)_N$.

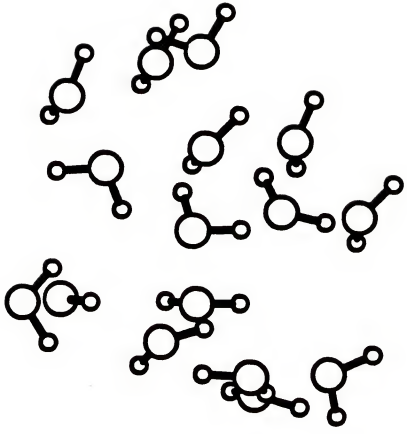

Figure 3.9 Structure of the microdroplet of water.

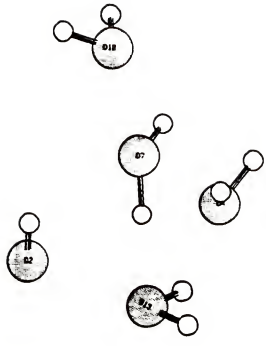

Figure 3.10 Structure of the water pentamer.

The interaction of positive ions with water is of importance in biochemistry. Many theoretical (65,66) and experimental studies (67) on the energetics of ionic solvation, particularly for the interaction of Na^+ and K^+ with water, are available in the literature. In the experimental investigations, the enthalpy for the stepwise addition of $(H_2O)_n$, n= 1, . . . , 6, to the sodium and potassium ions was measured. Cieplak et al (65) evaluate the interaction energies for these processes using a Monte Carlo technique. The potential function used in their studies include, in addition to the coulombic, R^{-6} and R^{-12} contributions, a term which

depends explicitly on the transfer of charge from the water molecules to the ion. Furthermore, a three body contribution to the interaction energy is also calculated.

Parameters for ionic solvation for the Fraga potential are available (51). The systematic hydration energy per water molecule for the stepwise solvation of the sodium and potassium ions were calculated using the annealing method. These results are given in Tables 3.9 and 3.10 (column 2) along with values obtained by Cieplak et al (65) in column 3. The corresponding experimental values which are given in column 4 have been obtained from the measured enthalpies corrected for the kinetic energy contribution.

TABLE 3.9 Interaction energies per water molecule (kcals/mole) for the sodium ion with (water)n

n	ΔE_1 (kcals/mole)	ΔE_1 (kcals/mole) (ref 65)	EXPERIMENT (kcals/mole) (ref 67)
1	-23.89	-23.01	-23.40
2	-25.30	-22.35	-21.30
3	-26.04	-20.43	-19.27
4	-26.69	-18.53	-17.93
5	-27.05	-17.24	-16.54
6	-27.39	-16.33	-15.47

TABLE 3.10 Interaction energies (kcals/mole) per water molecule for the potassium ion with (water)n

n	ΔE_1 (kcals/mole)	ΔE_1 (kcals/mole) (ref 65)	EXPERIMENT (kcals/mole) (ref 67)
1	-18.66	-17.80	-17.30
2	-20.07	-16.75	-16.41
3	-20.72	-15.70	-15.14
4	-21.36	-14.70	-14.16
5	-21.64	-13.84	-13.35
6	-21.87	-13.27	-12.69

The results in column 2 of Tables 3.9 and 3.10 clearly show the inadequacy of the Fraga potential energy function and its parameters in studying problems dealing with ionic solvation. Not only are the values overestimated, the trend in the values is completely opposite to that obtained from experiment.

The interaction energy for Na^+ and K^+ with one water molecule is in excellent agreement with the Monte Carlo value and experimental results. The positive charge on the ion is not going to remain localised on the ion after the first water molecule has coordinated; some of this charge will be reduced by the transfer of electron density from the ligand. Thus, the second water molecule is no longer interacting with a unipositive ion, but an ion with a reduced charge. The multipolar expansion, in the weak interaction limit, is not able to account for such charge transfer terms.

For the interaction of charged species, the coulombic term is certainly the dominant contribution to ΔE. As the reduction of the charge on the ion is neglected, the coulombic term is systematically overestimated. Although the short range repulsion term increases due to the increase in the number of water molecules, it cannot adequately compensate for the large negative coulombic contribution.

3.5 Discussion

The types of systems to which the simulated annealing method has been applied in this chapter are varied. The study includes clusters of polar and non polar molecules and ion-dipole interactions.

The success of the method depends on the quality of the potential energy function used. If more terms which describe the the nature of the interactions are included, the predictive power of the method is enhanced.

Within the polarisation approximation, the multipolar expansion of the interaction energy is exact only if the summation is to infinite order. However, it is necessary to truncate the series to a finite numer of terms as explained in Chapter 1. In the Fraga potential function, the four terms used to calculate ΔE are

1. the coulombic or long range term that is a function of R^{-1},
2. a medium range term which decays according to R^{-4},
3. the short range dispersion term which behaves as the inverse sixth power in R, and

4. the very short range repulsion term which is a function of R^{-12}.

The R^{-4} term takes into account the induction in a molecule caused by the field generated by the other molecules in the vicinity. Such a term is the leading term in the interaction of non-polar systems like benzene.The success of the method in obtaining the T-shaped structure for the benzene dimer is due to the inclusion of this term in the evaluation of the interaction energy.

For neutral, non-polar systems, the leading term that contributes to stabilisation is the dispersion term which depends on R^{-6} as its leading term and is difficult to obtain from calculations. Parameterisation of this term using the Slater-Kirkwood approximation (68) includes some of the dispersion effects.

The multipolar expansion is strictly valid only in the limit of large intersystem separation, R. Thus effects like charge transfer, which are short ranged phenomena, are not included. The predictive nature of potential functions based on this approximation for systems in which such effects are dominant is certainly questionable.. The results obtained for ionic hydration (Tables 3.9 and 3.10) illustrate the limitation of the Fraga potential. A careful study of the results show a need for the incorporation of the charge transfer and other short-range terms into the potential function before it can be used to examine ionic hydration.

The pairwise summation of the interaction fails to take three body and higher order effects into consideration. In the case of dipolar systems like water, such terms are important to account for the cooperativity and the clustering of the constituent molecules. Simulations of other thermodynamic properties like

free–energy changes and specific heats, especially for polar molecules, have been shown (69,70) to require the inclusion of such terms. in order to obtain reasonable agreement with experimental observations.

Application of the Fraga potential incorporated into the simulated annealing method has been particularly successful for large systems, as illustrated in the cluster formation of water and benzene. The microdroplet sizes predicted are in remarkable agreement with those obtained from the solvophobic theory.

The application of the simulated annealing method using the potential energy function given in equation (3.12) is successful in finding the global minimum of a molecular potential energy surface. Its sucessful application to a wide range of electronically neutral systems makes it particularly useful in finding the global minimum on the potential energy surface of solute-solvent interactions, thereby determining the structure of solvent molecules in the solvation shells surrounding the solute.

CHAPTER 4
ELECTRONIC SPECTRA USING THE DISCRETE-CONTINUUM SOLVENT MODEL

4.1 Introduction

The anisotropy of the solvent can be taken into account by assigning a structure to the molecules that form the solvent shells immediately surrounding the solute. These shells are referred to as the discrete structure of the solvent and the simulated annealing method described in the previous chapter is well suited in accomplishing this task. After the discrete solvent structure has been obtained, the energy of the solute-solvent cluster can be calculated using the supermolecule approach or the point charge approximation to the solvent. The first method has been outlined in chapter one. In the point charge model, the atoms in the solvent molecules can be approximated as point charges, having the same values as those used in the simulation. The effect of these charges can then be incorporated into the solute Hamiltonian H_s. The derivation of the solute–discrete solvent Hamiltonian, H_{S-D}, within the point charge approximation for the simulated solvent structure is given in section 4.2.

Multiphoton spectroscopy (MPS) (71) is an analytical method in which the spectrum of a molecule surrounded by a few solvent molecules can be obtained. The number of solvent molecules in such clusters is usually in the range of one

to six. Using the method presented in section 4.2, the electronic spectra of a series of such clusters have been calculated within the INDO approximation. The results, along with the corresponding MPS values are presented in section 4.3.

To describe the solvent completely, each discrete solvent cluster obtained from the simulated annealing method is centered in a cavity having a suitable radius, which is then embedded in the continuum solvent. The method used in the selection of a value for this radius is presented in section 4.4. The criterion for building the discrete solvent cluster is that one solvent molecule at a time is allowed to interact with the solute molecule. As more solvent molecules are added, the interaction energy per solvent molecule ΔE_1 converges to an average value. When the decrease in ΔE_1 is less than half a kilocalorie per mole, the cluster buildup is considered to be complete and the solvent molecules that form such a cluster is said to comprise the discrete solvent structure.

Treating the solute-solvent cluster as a modified solute, the continuum solvent effect is incorporated into H_{S_D} in the same manner as that presented in Chapter 2. This model is referred to as the discrete–continuum model and the results obtained using this model are tabulated in section 4.4. Conclusions based on the results presented in this chapter are given in the final section.

4.2 Derivation of the Hamiltonian for the Solute-Discrete Solvent System

Let the solute Hamiltonian be denoted H_s. Suppose the M atoms that comprise the N solvent molecules are replaced by point charges $\{ q_i \}$ at positions $\{ r_i \}$,

i = 1, 2, . . . , M. The charges q_i are the same values as those used in the simulated annealing method to obtain the structure of the solvent cluster.

H_{S-D}, the Hamiltonian for the interaction of the solute with the discrete solvent structure is given by

$$H_{S-D} = \frac{1}{2}\sum_{A}\sum_{i=1}^{M}\frac{Z_A q_i}{r_{iA}} - \frac{1}{2}\sum_{i=1}^{M}\sum_{j\in S}\frac{q_i}{r_{ij}} \qquad 4.1$$

The first term on the right hand side of the above equation is the attraction between the point charge q_i and the nuclear cores of the solute and the second term is the electron – electron interaction between the solute electrons j and the point charge. The summation index A represents the nuclei in the solute, Z_A is the core charge on center A and j runs over the electrons in the solute molecule S.

The Hamiltonian H^* for the composite solute-solvent shell system is given by

$$H^* = H_S + \frac{1}{2}\sum_{A\in S}\sum_{i=1}^{M}\frac{Z_A q_i}{r_{Ai}} - \frac{1}{2}\sum_{i=1}^{M}\sum_{j\in S}\frac{q_i}{r_{ij}} + \frac{1}{2}\sum_{i=1,j=1}^{M}\frac{q_i q_j}{r_{ij}} \qquad 4.2$$

The energy E^* is then given by

$$E^* = <\Psi|H^*|\Psi>$$

where Ψ is the normalised electronic wavefunction for the solute system. As q_i { i = 1, 2, . . . , M } does not depend on Ψ,

$$E^* = E_{Nuc,S} + \frac{1}{2}\sum_{A\in S}\sum_{i=1}^{M}\frac{Z_A q_i}{r_{Ai}} + \frac{1}{2}\sum_{i=1,j=1}^{M}\frac{q_i q_j}{r_{ij}}$$

$$+ <\Psi|H_S - \frac{1}{2}\sum_{i=1}^{M}\sum_{j\in S}\frac{q_i}{r_{ij}}|\Psi> \qquad 4.3$$

where $E_{Nuc,S}$ is the core repulsion energy of the solute. From the last term of equation 4.3, the effect of the point charges is to modify the one electron part of the solute Hamiltonian H_S according to

$$< \Psi | H_S - \frac{1}{2} \sum_{i=1}^{M} \sum_{j \in S} \frac{q_i}{r_{ij}} | \Psi > =$$

$$< \Psi | T - \frac{1}{2} \sum_{A \in S, j \in S} \frac{Z_A}{r_{jS}} - \frac{1}{2} \sum_{i=1}^{M} \sum_{j \in S} \frac{q_i}{r_{ij}} + G | \Psi >$$

where T is the kinetic energy operator of the electrons and G is the Fock potential. Modification of the one electron part of the solute Hamiltonian can be calculated as the penetration of the point charges into the atomic cores of the solute nuclei. It is this method, that is, the change of H_S due to the penetration integrals within the INDO formulation that is used in the calculations, the results of which are presented in the next section.

4.3 Electronic Spectra of a Solute with a Discrete Number of Solvent Molecules

The solvent induced shifts were calculted using the method presented in section 4.2. The origins for the shifts tabulated below, were the gas phase values calculated from INDO and those obtained experimentally. Each cluster was simulated as described in the introduction to this chapter, that is, by building the solvent shell, one molecule at a time till the interaction energy per solvent molecule converges to within half a kilocalorie per mole. The size of the active space in the configuration interaction procedure was restricted to ten orbitals,

five occupied and five unoccupied, the same space used in all the calculations presented in Chapter 2.

TABLE 4.1 Gas phase spectra of some solute molecules.

SYSTEM	CALCULATED TRANSITION (cm^{-1})	EXPERIMENTAL TRANSITION (cm^{-1})
phenol	36950	36352 (ref 37)
benzene	37974	38090 (ref 73)
pyrazine	29071	30875 (ref 77)
pyrimidine	33235	31073 (ref 24)

The first system investigated was the step-wise hydration of phenol and the results are given in Table 4.2.

TABLE 4.2 Shifts in the $\pi \rightarrow \pi^*$ transitions for phenol — $(H_2O)_n$ n = 1, 2, 3, 5

n	CALCULATED SHIFT (cm^{-1})	EXPERIMENTAL SHIFT (ref 37)(cm^{-1})
1	-123	-356
2	-225	-93
3	-196	-89
.	.	.
5	-99	.

Experimental results using the MPS techniques (37) show a red shift in the lowest $\pi \rightarrow \pi^*$ band of phenol when hydrated by one water molecule. This is due to the proton donor property of the central molecule resulting in the formation of the phenolate ion. The first water molecule is therefore expected to orient itself such that the phenolic hydrogen can bond to the oxygen atom of the water molecule. Figure 4.1 shows the structure of the phenol-water complex as calculated by the simulated annealing method. The arrangement of the solvent molecule clearly shows its proton acceptor property.

Further hydration by another molecule causes a blue shift, with respect to the lowest band of the phenol-water complex, in the experimental spectrum for the same $\pi \rightarrow \pi^*$ band as listed in Table 4.2. In this case the second water molecule stabilises the phenolate ion resulting in the observed shift as verified by Kasha et al (72). The additional solvent molecule should orient itself such that the hydrogen atoms now behave as proton donors.

The calculated spectral shifts show that two water molecules are necessary for the formation of the phenolate ion which is then stabilised by the third solvent molecule. It is therefore expected that two water molecules will behave as proton acceptors towards the phenol. Figures 4.2 and 4.3 show the phenol-$(H_2O)_2$ and phenol-$(H_2O)_3$ structures calculated by the annealing method. The orientation of the first two water molecules in figure 4.2 shows their acidic behaviour. In figure 4.3, the third water molecule is not in the immediate vicinity of the phenolic group. Spectroscopic evidence summarized in Table 4.2, shows that the spectral

shift due to this water molecule is small, and, it has been postulated (37), that only two water molecules are closely associated with the phenol molecule, the other water begins to form part of the bulk solvent, a result reproduced by the annealing method. The blue shift in the spectrum continues with increasing hydration,as the results for phenol-$(H_2O)_5$ indicate.

The orientations of the first three water molecules around the phenol are given in Figures 4.1, 4.2 and 4.3.

MPS studies of the interaction of benzene and diaza compounds with small molecules have been reported recently (74–77). For the interaction of benzene with one molecule of water and ammonia, the calculated interaction energy using the annealing method and shifts in the $\pi \rightarrow \pi^*$spectrum are given in Table 4.3 along with the experimental values for the shifts . The geometry of the ammonia molecule was taken from reference (78).

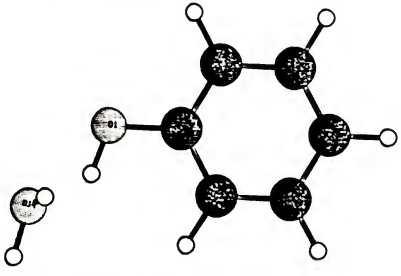

Figure 4.1 Orientation of H_2O around phenol.

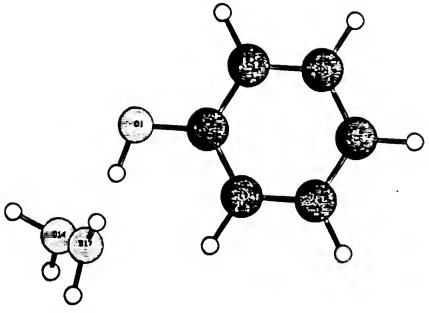

Figure 4.2 Structure of phenol – $(H_2O)_2$.

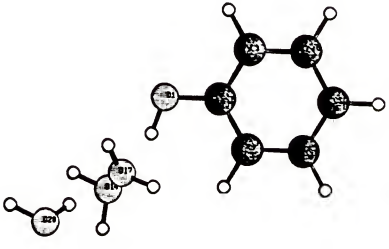

Figure 4.3 Arrangement of $(H_2O)_3$ around phenol.

TABLE 4.3 Calculated and experimental shifts for benzene with H_2O and NH_3.

SYSTEM	INTERACTION ENERGY (kcals/mole)	CALCULATED SHIFT (cm^{-1})	EXPERIMENTAL SHIFT (cm^{-1})
Benzene - H_2O	-2.66	0	78 (ref 75)
Benzene - NH_3	-4.49	0	-20 - +20 (ref 75)

Figure 3.4 shows the structure of the benzene-H_2O complex. The orientation of the ammonia molecule over the hydrocarbon is very similar to the former case, a near symmetrical arrangement. Thus, no change in the electric dipole moment is predicted and hence no spectral shift can be calculated.

Pyrazine interacting with NH_3 and $[CH_4]_n$, {n = 1, 2, 3} was investigated next. For pyrazine/$[CH_4]_2$ experimental studies (74) show two $n \rightarrow \pi^*$ peaks, one corresponding to the isotropic structure in which the two methane molecules are on either side of the pyrazine ring, and the other peak due to the anisotropic arrangement of the methane molecules. The simulated annealing method could not predict the isotropic structure for this system although it is expected to be the more stable one. The shifts in the $n \rightarrow \pi^*$ transition peaks and the calculated interaction energies are tabulated below.

TABLE 4.4 Interaction energies and shifts in the $n \rightarrow \pi^*$ transition peaks for pyrazine with NH_3 and methane.

SYSTEM	INTERACTION ENERGY (kcals/mole)	CALCULATED SHIFT (cm^{-1})	EXPERIMENTAL SHIFT (cm^{-1}) (ref 76)
pyrazine - NH_3	-5.54	-15	117
pyrazine - CH_4	-1.19	-7	-32
pyrazine - $(CH_4)_2$	-2.86	-9	-38
pyrazine - $(CH_4)_3$	-5.01	-21	-70

Figure 4.4 shows the position of the NH_3 molecule with respect to the pyrazine ring.

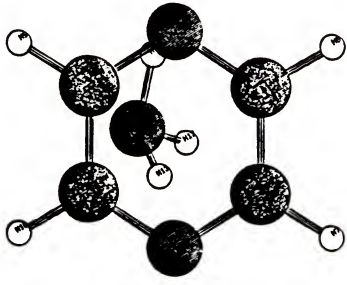

Figure 4.4 Position of NH_3 above the pyrazine ring.

Pyrimidine interacting with NH_3 and methane was the other systems studied. One of the differences between this system and the pyrazine / $[CH_4]_2$ is that both, the isotropic and anisotropic structures for its interaction with methane were calculated. The interaction energies and the shifts in the $n \rightarrow \pi^*$ transitions are given in Table 4.5

.

TABLE 4.5 Interaction energies and shifts in the $n \rightarrow \pi^*$ transition peaks for pyrimidine with NH_3 and methane.

SYSTEM	INTERACTION ENERGY (kcals/mole)	CALCULATED SHIFT (cm^{-1})	EXPERIMENTAL SHIFT (cm^{-1}) (ref 74)
pyrimidine - NH_3	-6.13	225	285
pyrimidine - CH_4	-1.18	33	-57
pyrimidine - $(CH_4)_2$ (iso)	-2.37	75	-112
pyrimidine - $(CH_4)_2$ (aniso)	-1.75	31	-47

The anisotropic and isotropic structures of pyrimidine with $[CH_4]_2$ are shown in Figures 4.5 and 4.6 respectively.

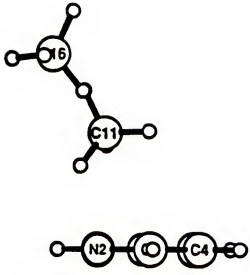

Figure 4.5 Anisotropic structure of pyrimidine – $(CH_4)_2$.

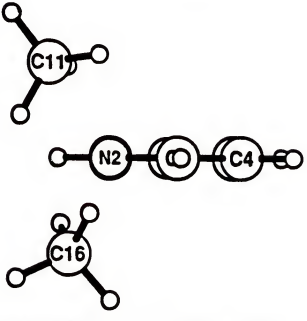

Figure 4.6 Isotropic structure of pyrimidine – $(CH_4)_2$.

The experimental shifts for the systems studied in Tables 4.3, 4.4 and 4.5 are small, and can be due to geometry changes in the central molecule due to the

solvent interactions. Such changes have been ignored in the calculations presented here. The emphasis in calculating these shifts is to investigate the power of the INDO method in predicting the direction of the shifts, that is, towards the red or blue side of that of the central molecule.

The calculations for the pyrazine-methane clusters reproduce the experimental shifts and the correct trend with increasing number of methane molecules. However, the shift calculated for the pyrazine-ammonia is opposite to the experimental observation. In the case of pyrimidine (Table 4.5), the trend is opposite — the shift for the pyrimidine-NH_3 complex is calculated in accordance with experiment whereas the pyrimidine-methane complexes are predicted to have blue shifts. Increasing the size of the configuration interaction space to twenty molecular orbitals, ten occupied and ten unoccupied, produced the same trend in the results.

The method fails for clusters in which the solute/solvent systems comprise polar/nonpolar molcular combinations. The hydrogen bonding capabilities of diazines in their excited states has been experimentally verified (75,79). In cases like pyrazine with NH_3, the method used to calculate the spectral shifts should be able to describe such intermolecular hydrogen bonding. which stabilises the excited state. The extent of the stabilisation may be small, but is indeed important in the calculations as the shifts measured are less than 250 wavenumbers. Replacing the solvent molecule by point charges removes any molecular properties the solvent may have, which in turn neglects specific intermolecular effects (76).

4.4 Shifts in the Electronic Spectra of a Solute Using the Discrete-Continuum Model

Using equation (4.1) and the continuum method presented in Chapter 2, the Hamiltonian H' for the solute – discrete solvent complex, centered in a cavity of radius ' b ' in the continuum solvent is now given by

$$H^{\bullet} = H_S - \frac{1}{2}\sum_{A}\sum_{i=1}^{N}\frac{Z_A q_i}{r_{iA}} + \frac{1}{2}\sum_{i=1}^{N}\sum_{j\in S}\frac{q_i}{r_{ij}}$$

$$-\frac{\hat{\mu}}{b^3}\left\{\frac{2(\epsilon-1)}{(\epsilon+2)} - \frac{(n^2-1)}{(n^2+1)}\right\}.\hat{\mu} \qquad 4.4$$

In order to treat the solute – discrete solvent cluster within the continuum model, a value for the radius of the cavity which contains the cluster is required. Two methods were used to evaluate this quantity — one was to calculate the radius r_{MD} as 1.5 times the radius obtained from the mass density as explained in Chapter 2. The other method was to take the maximum and minimum distances, r_{max} and r_{min}, of the center of mass of the solvent molecules from the origin. Once the value for the radius has been determined, the spectra can be calculated using the Hamiltonian given in equation (4.4) and the continuum solvent model detailed in Chapter 2.

The calculated and experimental values for the shifts in the spectral transitions for pyridine /$[H_2O]_n$ {n = 1, 2, 4 and 6} for the various values for the cavity radius are given in Table 4.6.

TABLE 4.6 Cavity radii and shifts in the $\pi \rightarrow \pi^*$ spectra for pyridine / $(H_2O)_n$ n = 1, 2, 4 and 6

SYSTEM	CAVITY RADIUS (A)	CALCULATED SHIFT (cm^{-1})	EXPERIMENTAL SHIFT (cm^{-1})
pyridine/H_2O	r_{MD} = 4.76	-94	
	r_{max} = r_{min}= 3.78	2830	
pyridine/$(H_2O)_2$	r_{MD} = 4.76	-147	
	r_{max}= 4.39	512	
	r_{min} = 4.20	219	
pyridine /$(H_2O)_4$	r_{MD} = 4.76	-125	
	r_{max}= 6.26	139	
	r_{min} = 5.38	-317	
pyridine/$(H_2O)_6$	r_{MD} = 4.76	346	
	r_{max} = 16.06	4	
	r_{min}= 12.76	9	
pyridine/water			713 (ref 28)

The results of a similar treatment for phenol/$(H_2O)_n$ {n = 1, 2, 3} are given in Table 4.7. The calculated shifts in the spectral transitions for the phenol/H_2O system using the distance from the solute origin to the center of mass of the solvent molecule as the cavity radius is ridiculous, the π^* state is predicted to have a dipole moment of 224 D. A similar result is obtained for the phenol/$(H_2O)_2$ system. It was therefore decided to use the scaled radius obtained from mass density measurements as explained in Chapter 2.

TABLE 4.7 Shifts in the $\pi \rightarrow \pi^*$ spectrum for phenol / $(H_2O)_n$ n = 1, 2, 3, 5

SYSTEM	CALCULATED SHIFT (cm^{-1})	EXPERIMENTAL SHIFT (cm^{-1})
phenol/H_2O	-66	
phenol / $(H_2O)_2$	-192	
phenol/$(H_2O)_3$	-152	
phenol/$(H_2O)_5$	29	
phenol/water		685 (ref 33)

From the results in Tables 4.6, the best value for the cavity radius is that obtained from mass density measurements. It was therefore decided to use this values for each of the solutes studied using this model.

In the case of pyridine with hexane and ethanol, the cluster buildup was performed using the simulated annealing method. In each instance, one solvent molecule was found to satisfy the criterion for the convergence of the interaction energy of the cluster.

TABLE 4.8 Shifts in the $\pi \rightarrow \pi^*$ spectral transitions using the discrete-continuum approach.

SYSTEM	CALCULATED SHIFT(cm^{-1})	EXPERIMENTAL SHIFT (cm^{-1})
pyridine/water	346	713 (ref 28)
pyridine/hexane	24	1491 (ref 30)
pyridine/ethanol	307	560 (ref 29)
phenol/water	29	685 (ref 33)

4.5 Conclusions

Simulation of solvent clusters around the nitrophenols could not be carried out as no parameters are available for the nitrogen atom in the nitro group.

The agreement between the calculated and experimental shifts presented in Table 4.8 is poor, although the discrete – continuum model is expected to be a better description of the solvent than the continuum model alone. Nevertheless, the calculated shift for pyridine in water has improved compared to the value of 290 wavenumbers obtained for the continuum model. For the other cases, however, there is no improvement.

In these calculations, the solute molecule was considered to be a monomer, an assumption that may not be valid for solutes where strong associations such as hydrogen bonding are possible. Phenol is an example of a molecule that exists as dimers and trimers in water (37). Furthermore, phenol which exhibits acidic behaviour in water, exists as a mixture of phenol and the phenolate ion, an effect not considered in the calculations. Experimental values for these shifts are a source of controversy in the literature as the purity of the solvent water is extremely important.

As explained in Chapter 2, the calculated spectral shifts are dependent on the value of the cavity radius. The method that was used to evaluate this parameter is the same for all the solute molecules. Such an approach may not be useful and it is therefore necessary to be able to define a cavity for the solute which has a

more realistic shape and suitable dimensions. In the following chapter, such an algorithm and the results of its applications are presented.

CHAPTER 5
AN ALGORITHM FOR A MORE REALISTIC DESCRIPTION OF THE SOLUTE MOLECULE

5.1 Introduction

In Chapters 2 and 4, the solute molecule was assumed to be a point dipole centered in a spherical cavity having a suitable radius. Very few molecules can be considered to be even approximately spherical in shape and, if its structure has side chains, the spherical cavity model is certainly a poor description of the solute. Furthermore, in studying processes like molecular dissociation, it is unrealistic to have the molecular fragments in a single spherical cavity surrounded by the solvent.

It is therefore necessary to determine a more realistic shape for the molecular cavity, and the algorithm that has been used in this chapter is based on the method presented by Miertus et al (80, 81). The molecular systems studied are the dissociation of HF and the hydration of the neurotransmitter γ – amino butyric acid (GABA).

5.2 Mathematical Formulation of the Algorithm

According to the method of Miertus et al, every atom in the solute molecule is centered in a sphere having the van der Waals radius of that particular atom. The cavity that surrounds the solute molecule is thus approximated as a set of interlocking spheres.

Suppose the solute molecule has a gas phase charge distribution ρ^0 corresponding to the Hamiltonian H_0. When this solute is immersed in a solvent having a dielectric constant ϵ, ρ_0 would induce a set of image charges $\{ q_i^0 \}$, i = 1, 2, ..., N, on the surfaces of the interlocking spheres which define the boundary of the cavity. The value of these charges will depend on the value of the dielectric constant — higher the value of ϵ, larger the magnitude of the charge. The number of such charges, N, is predetermined by the user.

These image charges will polarise each other resulting in a new set of charges $\{ q_i' \}$ and the solute molecule will experience the effect of these modified charges. Thus, the new Hamiltonian for the solute is H' where

$$H' = H_0 + V \qquad 5.1$$

where V is the effect of the image charges. The new charge distribution ρ' corresponding to H' will now induce image charges $\{ q_i'' \}$ which effects H' in a manner very similar to that of ρ^0 on H_0. This process of modifying the gas phase Hamiltonian of the solute using the influence of the induced image charges, V, is repeated until self–consistency in the total energy of the solute with respect to the Hamiltonian H' is obtained.

As a first step in applying this algorithm, an initial set of point charges $\{ q_i^0 \}$ i = 1, 2, ... N , is required. These charges which are located on the surfaces of the spheres are associated with the net charge q_A and the van der Waals radius r_A of the particular atom A on which the sphere is centered. The surface charge density σ_j^0 at the center of the surface element j on the sphere

centered on atom A is given by (82)

$$\sigma_j^0 = -\frac{(\epsilon - 1)}{\epsilon r_A^3} q_A / N_A \qquad 5.2$$

where N_A is the number of point charges around atom A. The charges q_j^0 are now given by

$$q_j^o = \sigma_j^0 \Delta S_j \qquad 5.3$$

where ΔS_j is the element of surface area associated with q_j^0 given by

$$\Delta S_j = 2r_A^2 \sin\theta_{A,j} \sin(\Delta\theta/2)\,\Delta\phi \qquad 5.4$$

$\theta_{A,j}$ is the angle made by the radius of the sphere to the center of the surface element under consideration with the positive z-axis, and $\Delta\theta$ and $\Delta\phi$ are the increments in the spherical angular coordinates that describe the sphere. In order that the surface elements have the same area at axial and equatorial positions, the increment in the angle ϕ, $\Delta\phi$, is calculated as a function of the angle θ and $\Delta\theta$ according to

$$\Delta\varphi = \frac{\Delta\theta}{\sin\theta} \qquad 5.5$$

Substituting equation (5.5) in (5.4) yields

$$\Delta S_j = 2r_A^2 \sin(\Delta\theta/2)\,\Delta\theta \qquad 5.6$$

Thus, for a given increment of $\Delta\theta$, equal areas are evaluated on the surface of the van der Waals spheres and at the center of each of these elements is located a point charge q_j^0 calculated according to equations (5.2) and (5.3).

The polarisation of each image charge q_j^0 in the presence of all the charges is evaluted next as the sum of two effects — one due to the presence of all the other point charges except itself and the other contribution attributed to the self-polarisation of q_j^0 whose effect is to reduce the magnitude of the charge.

The first effect is calculated using a finite difference method. The gradient of the potential between point charges q_j^0 and q_i^0, i not being equal to j, is evaluated as the difference in the potential at points r_i and $r_i + \delta$, where $|\delta|$ was arbitrarily chosen to be 0.01 A. The self-polarisation term was then evaluated taking into account the curvature of the sphere and, the process of charge polarisation is repeated till the charge distribution has converged within a predetermined threshold value. The equation used is

$$q_j^{0m} = q_j^0 - \frac{\epsilon - 1}{4\pi\epsilon}\left(\left\{\frac{\Delta S_j}{|\delta|}\sum_{i=/j} q_i^o\left[|r_j + \delta - r_i|^{-1} - |r_j - r_i|\right]\right\} - 2\pi q_j^0\left[1 - \left(\frac{\Delta S_j}{4\pi r_A^2}\right)^{-\frac{1}{2}}\right]\right) \qquad 5.7$$

r_j and r_i are the position vectors of the image charges j and i respectively and m is the number of cycles required for convergence.

The effect of the point charges, V, which modifies the Hamiltonian H_0 according to equation (5.1) is defined by

$$V = \sum_k \sum_{i=1}^{N} \frac{q_i^* Z_k}{(r_i - r_k)} - \sum_j \sum_{i=1}^{N} \frac{q_i^*}{(r_i - r_j)} \qquad 5.8$$

The summation index k runs over all atomic cores of charge Z_k and j represents the electrons in the solute. $\{q_i^*\}$ are the polarised image charges on the surface

of the Van der Waals spheres. The effect of V, as defined in the above equation, is to modify the one electron part of the solute Hamiltonian H_0.

In defining the Van der Waals spheres around each atom, the tail of the charge distribution $\rho(r)$ of the solute molecule will lie outside the boundary of the cavity. As a result of this truncation, the sum of all the image charges $\{ q_i^{\bullet} \}$ will not be zero. It is therefore necessary to normalise these point charges. We choose

$$q_{i,+}^{\bullet} = q_{i,+}^{\bullet} \left(1 - \frac{\sum_{i=1}^{N} q_{i,+}^{\bullet}}{Q} \right)$$

$$q_{i,-}^{\bullet} = q_{1,-}^{\bullet} \left(1 + \frac{\sum_{i=1}^{N} q_{i,-}^{\bullet}}{Q} \right)$$

where Q is the sum of the absolute values of the image charges and $q_{i,+}$ and $q_{i,-}$ represent the positive and negative charges respectively.

The method outlined above is incorporated into the INDO method (12, 13) and the results obtained are presented in the next section.

5.3 Results and Discussion of the Applications of the Point Charge Model

The first system studied was the dissociation of HF in water. Gas phase dissociation favours the homolytic cleavage of the HF bond (83) resulting in the formation of H and F radicals while heterolytic fission is observed in polar solvents. Previous work on this system (20) used the reaction field theory of

Onsager in which both atoms are in the same spherical cavity as the bond distance increased. The radius of the cavity did not change as a function of the distance between the H and F atoms.

In the calculations presented here, the total number of point charges on the cavity, N, and the increment $\Delta\theta$ in the spherical angle θ is varied. The energy E (in a.u.) and the formal charges on the atoms are evaluated as a function of the interatomic distance. In Table 5.1, the energy as a function of the interatomic distance is tabulated. Table 5.2 gives the formal charge on the hydrogen atom, δ_H, as a function of the bond distance and Figure 5.1 shows the potential energy curve for the dissociation of HF in water.

TABLE 5.1 Energy of HF (a.u.) as a function of the interatomic distance r, N and increment in the spherical angle.

r_{HF} (A)	GAS PHASE	N = 10, $\Delta\theta$ = 10	N = 100, $\Delta\theta$ = 10	N = 200, $\Delta\theta$ = 5	N = 240, $\Delta\theta$ = 5
0.5	-24.23971	-24.29171	-24.40536	-24.47807	-24.45333
0.7	-25.51578				-26.32725
0.8	-25.74363	-25.79341	-26.22123	-26.42758	-26.32314
1.0	-25.85487	-25.90582	-26.17718	-26.10647	-26.08222
1.2	25.77653				-26.00378
1.5	-25.59443	-25.71323	-25.99364	-25.79994	-25.82210
2.0	-25.37826	-25.59435	-25.77315	-25.71218	-25.73283
2.5	-25.27624	-25.52577	-25.58584	-25.63215	-25.65395
3.0	-25.22995	-25.72313	-25.84482	-25.783427	-25.80822
4.0	-25.19369	-25.89520	-25.93880	-25.94534	-25.96936

TABLE 5.2 Formal charge on the hydrogen atom as a function of the bond distance r.

r_{HF} (A)	N = 10, $\Delta\theta$ = 10	N = 100, $\Delta\theta$ = 10	N = 200, $\Delta\theta$ = 5	N = 240, $\Delta\theta$ = 5
0.5	0.744	0.808	0.803	0.799
0.8	0.479	0.508	0.573	0.564
1.0	0.421	0.522	0.504	0.499
1.5	0.541	0.753	0.604	0.625
2.0	0.733	0.884	0.843	0.861
2.5	0.822	0.891	0.929	0.943
3.0	0.996	0.999	0.998	0.998
4.0	1.000	1.000	1.000	1.000

The results in Table 5.2 clearly show that the strong dielectric nature of the solvent favors the formation of the proton and fluoride ion. The accumulation of charge on the atoms increases dramatically for values of the bond distance greater than 1.5 A. When the interatomic distance is 2.5 A, the molecule is almost completely dissociated, and at 4A, the proton and the flouride ion are the species found in aqueous solution. The increase in the energy when the bond distance is about 2.5 A is due to the heat of hydration, an effect observed by Karelson et al (20).

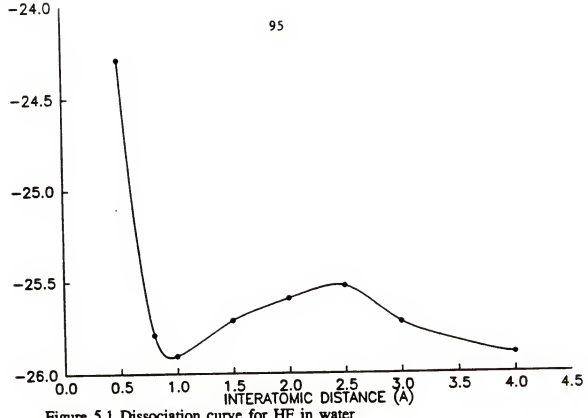

Figure 5.1 Dissociation curve for HF in water

The neurotransmitter γ–aminobutyric acid (GABA) was studied next. In polar solvents the zwitterionic structure $H_3N^+(CH_2)_3COO^-$ is observed as the solvent can stabilise the charge separated structure. The charge densities on the carboxylic carbon atom, denoted $\rho(C_1)$ and nitrogen atom, $\rho(N)$ were calculated for the zwitterion as a function of the number of image points N, and increment $\Delta\theta$ in the spherical angle θ using the method presented in this chapter. The results are given in Table 5.3

TABLE 5.3 Charge densities on the carboxylic carbon and nitrogen atoms of GABA.

	GAS PHASE	N = 16, $\Delta\theta$ = 30	N = 32, $\Delta\theta$ = 10	N = 48, $\Delta\theta$ = 10	N = 64, $\Delta\theta$ = 10	N = 160, $\Delta\theta$ = 10
Energy (a.u.)	-75.9005	-76.5136	-77.2897	-77.1395	-77.1946	-77.1384
$\rho(C_1)$	0.444	0.408	0.352	0.363	0.380	0.391
$\rho(N)$	-0.317	-0.282	-0.289	-0.292	-0.294	-0.293

The positive nature of the carboxylic carbon is reduced as the number of image charge points increase as is the negative charge density on the nitrogen atom.

The energies of GABA and its zwitterion in the gas phase and water calculated using the algorithm presented in this chapter are given below.

TABLE 5.4 Energies (a.u.) of GABA and its zwitterion.

	GAS PHASE	SOLVATED N=160, $\Delta\theta$ = 5
GABA	-76.0419	-76.2645
zwitterionic form	-75.9004	-77.1383

The above results indicate that the zwitterionic structure is more stable in water than GABA itself in accordance with experiment. This is to be expected as water being a polar solvent can stabilise the charge separated structure. In gas phase ths observation is reversed as no medium is available for the stabilisation of the charges in the zwitterion.

This result is certainly gratifying as a method as simple as that presented in this chapter is able to reproduce experimental observations. In a previous study if GABA and its zwitterion using the Onsager cavity model (84), the reaction field factor had to be manipulated in order to get results which agree with experiment.

The method presented in this chapter will not be able to show the formation of the zwitterionic structure as the explicit nature of the solvent molecules and the electronic processes involved in intermolecular interactions will have to be considered explicitly. Such a treatment requires supermolecular calculations and have been reported by Purvis and Zerner(85).

An algorithm which divides the surface area of the sphere into equal segments and determines the increase in the spherical angle ϕ as a function of θ is one way in which the method presented here can be improved.

CHAPTER 6
CONCLUSIONS

The results of the calculations presented in this thesis have been discussed in detail in the relevant sections in the preceeding chapters. Only general comments on the applicability of the methods and the theory used will be presented here.

In spite of its inherent assumptions, the reaction field method has been shown to be useful in obtaining solvent induced spectral shifts for a series of molecules. In those cases where strong interactions between the solute and the solvent exist, for example, pyridine in water, the method is not expected to be successful. The theory on which the method is based , that of weak solute–solvent interactions, neglects any change in the chemical structure of the constituent systems. Thus, phenomena, like the formation of a pyridinium ion, cannot be adequately described using the reaction field method.

A drawback in the method is that the results are dependent on the value of the cavity radius, as the solvent perturbation, that is, the reaction field term is inversely proportional to the cube of this parameter. If the radius is too small, the effect of the solvent is overestimated; too large a value will not include the solvent effects in any meaningful manner, thereby reproducing the vacuum state properties of the solute. It is reasonable to expect that any algorithm that is used to calculate the value for the cavity radius should include some phsical property of the solute. However, recent studies using a multiconfigurational selfconsistent reaction field technique

(86) have shown that properties, like the ionisation potential of a solvated molecule, can be evaluated with resonable accuracy using the reaction field scheme.

The continuum solvent model assumes the solute to be a monomer at infinite dilution. Experimentally this may not be the case as the entity whose spectra is being measured could be an associated form of the solute, an effect which is important in dealing with solutes with hydrogen bonding capabilities.

The success of the simulated annealing method using the Fraga intermolecular potential energy function and the limitations in its applicability have been demonstrated in Chapter 3. As the annealing parameter T^* has units of energy and not temperature, the simulated annealing method is well suited for incorporation into standard quantum chemical methods used in evaluating molecular properties.

From a computational point of view, the time required to evaluate minima is somewhat longer than in a gradient search technique, as the annealing algorithm has to be given an adequate number of moves and cycles in order to ensure that the potential energy surface has been scanned as completely as possible. However, the advantage is that, given these conditions, the global minimum is reached as explained in Chapter 3.

The discrete–continuum model for the solvent includes the anisotropy of the solvation shells and the bulk effects of the solvent. The formation of the solvent cluster is time consuming, especially for larger solvent molecules with conformational flexibilty as in the case of ethanol and hexane. In the calculations presented

in chapter 4 for pyridine in ethanol and hexane such conformational effects were not considered.

Recent spectroscopic studies have been reported for the stepwise solvation of tryptophan and other indole derivatives (87). The formation of the solvent shells would favour a buildup around the saturated side chains and therefore, the effect on the π sytem will be very small. The method, as presented in this dissertation is not expected to be able to evalute the spectral shifts in such cases with any reasonable accuracy.

Some improvements to the methods will now be presented. A better algorithm for the calculation of the cavity radius is required. The method should not be time consuming, and, furthermore, need not be solely dependent on the solute properties. Inclusion of some of some solvent parameters like the surface tension seems reasonable from physical considerations. The dispersion term and the effects of the polarisation of the solute by the solvent will have to be considered explicitly so as to make the reaction field method applicable to both polar and nonpolar systems.

The success of the intermolecular potential function used here in treating neutral systems has been previously emphasised. However, in order to study charged systems and molecules with a large separation of charges, like zwitterions, another function which explicitly considers the interactions in such systems will have to be used.

The defining of a more realistic shape for the solute cavity in terms of

interlocking van der Waals spheres makes it possible to study a wider range of molecules, specially those with side chains. The results obtained will be dependent on the values of the radii used for these spheres.

The results presented in this thesis demonstrate that it is indeed possible to construct simple and useful models for solvents without resorting to expensive supermolecular calculations whose applicability is severely restricted by the size of the constituent molecules. The incorporation of the solvent effects into the Hamiltonian for the solute can be done in various physically meaningful ways and this flexibility is very helpful in studying problems dealing with solvation.

APPENDIX
THE REACTION FIELD METHOD

In this method, the solvent molcules are replaced by a continuum and the solute is treated as a polarisable dipole centered in a cavity which is embedded in the continuum. For purposes of simplicity, the cavity is assumed to be a sphere of radius ' a '. As the solute is neutral, the potential in the cavity can be obtained by solving Laplace's equation. Without loss of generality, the z–axis is taken to be the direction of the dipole, the origin of the system of axes being coincident with the center O of the sphere.

As the system has spherical symmetry, the ϕ dependence of the potential will not appear explicitly in the expression for the potential V. Thus V can be regarded as a function of the variables r and θ.

Let V_1 and V_2 be the potentials outside and inside the cavity respectively. As the solute and solvent molecules are neutral, there are no excess charges present. Therefore V_1 and V_2 satisfy the Laplace equation

$$\Delta V_1 = 0 \qquad A.1$$

$$\Delta V_2 = 0 \qquad A.2$$

Suppose a general potential $V(\ r,\theta\ )$ which satisfies the Laplace equation is separable according to

$$V(r,\theta) = R(r)\,\Theta(\theta) \qquad A.3$$

The Laplace equation is given in spherical polar coordinates by

$$\Delta V = \frac{1}{r}\frac{\partial}{\partial r}\left(r\frac{\partial V}{\partial r}\right) + \frac{1}{r^2}\frac{\partial^2 V}{\partial \theta^2} = 0 \qquad A.4$$

Substituting equation (A.3) in (A.4) followed by separation of variables yields

$$\frac{r}{R(r)}\frac{d}{dr}\left(r\frac{dR(r)}{dr}\right) = -\frac{1}{\Theta(\theta)}\frac{d^2\Theta}{d\theta^2} = \lambda \qquad A.5$$

where λ is the constant of separation.

The Θ part of equation (A.5) is

$$\frac{d^2\Theta}{d\theta^2} = -\lambda\Theta$$

whose solution is given by

$$\Theta = A\cos\left(\sqrt{\lambda}\theta\right) + B\sin\left(\sqrt{\lambda}\theta\right) \qquad A.6$$

where A and B are constants. Using the periodic properties of the function $\Theta(\theta)$ in equation (A.6) yields

$$\lambda = n^2 \qquad n = 0, 1, 2, \ldots$$

Thus,

$$\Theta = A\cos(n\theta) + B\sin(n\theta) \qquad A.7$$

The function $\Theta(\theta)$ can be written in terms of the Legendre polynomials in $\mathrm{Cos}(\theta)$, $P_n(Cos(\theta))$.

The radial part of equation (A.5) now reads

$$r^2\frac{d^2R(r)}{dr^2} + r\frac{dR(r)}{dr} - n^2R(r) = 0 \qquad A.8$$

which is an Euler equation and its solution is given by

$$R(r) = c_1r^n + c_2r^{-n} \qquad A.9$$

Inserting equations (A.8) and (A.9) in (A.3) and using the principle of linear superposition, one obtains

$$V = \sum_{n=0}^{\infty} \left(L_n r^n + \frac{M_n}{r^n} \right) P_n(\cos\theta) \qquad A.10$$

The constants L_n and M_n incorporate A, B, c_1 and c_2.

Solution for the potential outside and inside the cavity.

The potentials V_1 and V_2 outside and inside the cavity are given by:

$$V_1(r) = \sum_{n=0}^{\infty} \left(L_n^{(1)}(r) + \frac{M_n^{(1)}}{r^{n+1}} \right) P_n(\cos\theta) \qquad A.11$$

$$V_2(r) = \sum_{n=0}^{\infty} \left(L_n^{(2)}(r) + \frac{M_n^{(2)}}{r^{n+2}} \right) P_n(\cos\theta) \qquad A.12$$

In order to determine the coefficients $L_n^{(i)}$, $M_n^{(i)}$, { i = 1, 2 }, boundary conditions on the potential are required. These conditions are:

$$[V_1(r)]_{r\to\infty} = 0 \qquad A.13$$

$$[V_1(r)]_{r=a} = [V_2(r)]_{r=a} \qquad A.14$$

$$\epsilon \left[\frac{\partial V_1(r)}{\partial r} \right]_{r=a} = \left[\frac{\partial V_2(r)}{\partial r} \right]_{r=a} \qquad A.15$$

where ϵ is the dielectric constant of the bulk fluid. The only source of charge inside the cavity is the dipole μ. Hence

$$V_2(r) = \frac{\mu}{r^2} \cos\theta \qquad A.16$$

where θ is the angle an arbitrary point in the cavity makes with the positive z-axis. Thus,

$$M_1^{(2)} = \mu \qquad A.17$$

and

$$M_n^{(2)} = 0 \qquad \forall n,\ (n \neq 2) \qquad A.18$$

Inserting equations A.17 and A.18 into A.12 yields

$$V_2(r) = \sum_{n=0}^{\infty} L_n^{(2)} r^n P_n(\cos\theta) + \frac{\mu}{r^2}\cos\theta \qquad A.19$$

From equation A.13, it is clear that in order to have a finite potential,

$$L_n^{(1)} = 0 \qquad \forall n$$

This simplifies $V_1(r)$ as

$$V_1(r) = \sum_{n=0}^{\infty} \frac{M_n^{(1)}}{r^{n+1}} P_n(\cos\theta) \qquad A.20$$

The Legendre polynomials are linearly independent. Using equations A.14 and A.15 in A.19 and A.20 yields

$$\frac{M_n^{(1)}}{a^{n+1}} = L_n^{(2)} \qquad n \neq 1$$

$$and \qquad A.21$$

$$-\epsilon(n+1)\frac{M_n^{(1)}}{a^{n+2}} = nL_n^{(2)}a^{n-1}$$

Equations A.21 are consistent if and only if

$$M_n^{(1)} = 0 \qquad n \neq 1$$

$$L_n^{(2)} = 0$$

For the special case when n = 1, equations A.19 and A.20 together with the boundary conditions yield

$$\frac{M_1^{(1)}}{a^2} = L_1^{(2)} a + \frac{\mu}{a^2} \qquad A.22$$

and

$$-2\epsilon \frac{M_1^{(1)}}{a^3} = L_1^{(2)} - \frac{2\mu}{a^3} \qquad A.23$$

$L_1^{(2)}$ and $M_1^{(1)}$ can now be obtained from these two equations as

$$L_1^{(2)} = -\frac{2(\epsilon - 1)\mu}{(2\epsilon + 1)a^3} \qquad A.24$$

and

$$M_1^{(1)} = \frac{3}{2\epsilon + 1}\mu \qquad A.25$$

Thus, the potentials outside and inside the cavity are given by

$$V_1(r) = \frac{3}{2\epsilon + 1}\frac{\mu}{r^2}\cos\theta \qquad A.26$$

and

$$V_2(r) = \frac{\mu}{r^2}\cos\theta - \frac{2(\epsilon - 1)}{2\epsilon + 1}\frac{\mu}{a^3} r\cos\theta \qquad A.27$$

From equation (A.27) , it is clear that the field inside the cavity is enhanced by a uniform field $\boldsymbol{R}$ given by

$$R = \frac{1}{a^3}\frac{2(\epsilon - 1)}{2\epsilon + 1}\mu \qquad A.28$$

This field is called the reaction field and is due to the the image created by the solute dipole in the surrounding continuum fluid.

REFERENCES

1. Berndt, M. & Kwiatkowski, J. S., "Theoretical Chemistry of Biological Systems," Ed. by G. Naray-Szabo, Studies in Physical and Theoretical Chemistry, Vol **41** Elsevier; Amsterdam (1986)

2. Beveridge, David L. & Schnuelle, Gary W., J. Phys. Chem. **79** 2562 (1975)

3. Noell, J. Oakley & Morokuma, Keiji, Chem. Phys. Lett **36** 465 (1975)

4. Kolos, W., Theoret. Chim. Acta. **51** 219 (1979)

5. Margenau, H. & Kestner, N. R ., "Theory of Intermolecular Forces," Chapter 2, Second Edition, Pergamon Press; New York (1971)

6. Jorgensen, W. L., Chandrasekhar, J., Madura, Jeffry D., Impey, Roger W. & Klein, Michael L., J. Chem. Phys. **79** 926 (1983)

7. Clementi, E., Cavallone, F. & Scordamaglia, R., J. Am. Chem. Soc. **99** 5531 (1977)

8. Woodward, R. B., J. Am. Chem. Soc. **63** 1123 (1941)

9. Woodward, R. B., J.Am. Chem. Soc. **64** 72, 76 (1942)

10. Pople, J. A., Beveridge, D. L., & Dobosh, P. A., J. Chem. Phys. **47** 2026 (1967)

11. Roothan, C. C. J., Rev. Mod. Phys. **23** 69 (1951)

12. Ridley, J. E. & Zerner, M. C., Theoret. Chim. Acta. **32** 111 (1973)

13. Bacon, A. D. & Zerner, M. C., Theoret. Chim. Acta. **53** 21 (1979)

14. Donnelly, R. A., Chem. Phys. Lett. **136** 274 (1987)

15. Onsager, L., J. Am. Chem. Soc **58** 1486 (1936)

16. Bayliss, N. S. & McRae, E. G., J. Phys. Chem. **58** 1002 (1954)

17. Bottcher, C. J. F., "Theory of Electric Polarization," Vol 1, Elsevier; Second Edition, Amsterdam (1973)

18. Amos, A. T. & Burrows, B. L., "Solvent – shift effects on electronic spectra and excited state dipole moments and polarisabilities," Advances in Quantum Chemistry, Vol 7, Ed. P.O.Lowdin, Academic Press, New York (1973).

19. Abe, T., Bull. Chem. Soc. Jap. **38** 1314 (1965)

20. Karelson, Mati M., Katritzky, Alan R. & Zerner, Michael C., Int. J. Quant. Chem. Symp. **20** 521 (1986)

21. Bondi, A., Physical properties of molecular crystals, liquids and glasses, pp 453 - 468, John Wiley, New York, (1968)

22. Handbook of Chemistry and Physics, 65th edition, CRC Press, Boca Raton, Florida, (1984)

23. Bekarek, Vojtech & Seccik, Juraj, Collect. Czech. Chem. Comm. **51** 746 (1986)

24. Innes, K. K. , Byrne, J. P. & Ross, I. G., J. Mol. Spectr. **22** 125 (1967)

25. Bist, H.D., Brand, J. C. D., & Williams, D. R., J. Mol. Spectr. **21** 76 (1966)

26. Trueblood, K. N., Goldfish, E. & Donohue, J., Acta Cryst **14** 1009 (1961)

27. Loppens, P., Schmidt, G. M. J., Acta Cryst **18** 654 (1965)

28. Cullis, P. M. & Wolfenden, R., Bioch **20** 3024 (1981)

29. Giacobbe, Thomas J., McGregor, Stanley D. & Beman, Floyd L., J. Het. Chem. **11** 889 (1974)

30. Ghersetti, S., Maccagnani, F., Mangini, A. & Montanari, F., J. Het. Chem. **6** 859 (1969)

31. Santavy, F., Walterova, D. & Hruba, L., Collect. Czech. Chem. Comm. **37** 1825 (1972)

32. Street, Jr. K.W. & Schenk, G.H., J. Pharm. Sci. **78** 1306 (1979)

33. Shizuka, Haruo, Toshifumi, Morita, Mori, Yugi & Tanaka, Ikuzu, Bull. Chem. Soc. Jap. **42** 1831 (1969)

34. Kalmus, C. E. & Hercules, D. M., J. Am. Chem. Soc. **96** 449 (1974)

35. Wheatly, P. J., Acta Cryst **10** 182 (1957)

36. Giller-Pandraud, H., Bull. Soc. Chim. Fr. **5th Ser.** 1988 (1967)

37. Kiyokazu, Fuke & Koji, Kaya, Chem. Phys. Lett. **94** 97 (1983)

38. Head, J. D. & Zerner, M. C., Chem. Phys. Lett. **131** 359 (1986)

39. Kirkpatrick, S., Gelatt, Jr. C. D. & Vecchi, M. P., Science **220** 671 (1983)

40. Kirkpatrick, S., J. Stat. Phys. **34** 975 (1984)

41. Donnelly, R. A., Chem. Phys. Lett. **136** 274 (1987)

42. Metropolis, N., Rosenbluth, Arianna W., Rosenbluth, Marshall N., Teller, Augusta, H. Teller, Edward, J. Chem. Phys. **21** 1087 (1953)

43. Rossky, Peter J. & Schnitker, Jurgen, J. Phys. Chem. **92** 4277 (1988)

44. Rossky, P. J., Ann. Rev. Phys. Chem. **36** 321 (1985)

45. Jorgensen, W. L., Chandrasekhar, J., Madura, Jeffry D., Impey, Roger W. & Klein, Michael L., J. Chem. Phys. **79** 926 (1983)

46. Bernal, J. D. & Fowler, R. H., J. Chem. Phys. **1** 515 (1933)

47. Fraga, S., J. Comp. Chem. **3** 329 (1982)

48. Clementi, E., Int. J. Quant. Chem. **3S** 179 (1969)

49. Clementi, E., Cavallone, F. & Scordamaglia, R., J. Am. Chem. Soc. **99** 5545 (1977)

50. Fraga, S., Saxena, K. M. S. & Karwowski, J., Hartree-Fock Atomic Data, Elsevier, Amsterdam (1975)

51. Nilar, S. H. M. & Fraga, S., J. Comp. Chem. **5** 261 (1984)

52. Kuchitsu, K. & Bartell, L. S., J. Chem. Phys. **36** 2460 (1962)

53. Curtiss, L. A., Frurip, D. J. & Blander, M., J. Chem. Phys. **71** 2703 (1979)

54. Odutola, J. A., Dyke, T. R., J. Chem. Phys. **72** 5062 (1980)

55. Anders, Engdahl & Bengt, Nelander, J. Chem. Phys. **86** 4831 (1987)

56. Campbell, Edwin S. & Belford, David, Theoret. Chim. Acta. (Berl) **61** 295 (1982)

57. Brodskaya, E. N. & Rusano,v A. I., Mol. Phys. **62** 251 (1987)

58. Plummer, P. L. Moore & Chen, T. S., J. Chem. Phys. **86** 7149 (1987)

59. Karlstroem, G., Linse, P., Wallqvist, A., Joensson, B., J. Am. Chem. Soc. **105** 3777 (1983)

60. Sinanoglu, O., J. Chem. Phys. **75** 463 (1981)

61. Kiermeier, A., Ernstberger, B., Neusser, H. J. & Schlag, E. W., J. Phys. Chem. **92** 3785 (1988)

62. Cullen, J. M., Ph. D. Thesis, University of Guelph, Canada (1981)

63. Carsky, P., Selzle, H.L., & Schlag, E. W., Chem. Phys. **125** 165 (1988)

64. Hermansson, Kersti, J. Chem. Phys. **89** 2149 (1988)

65. Cieplak, Poitr, Lybrand, Terry P. & Kollman, Peter A., J. Chem. Phys. **86** 6393 (1987)

66. Abraham, Farid F., Mruzik, Michael R. & Pound, G. Marshall, J. Chem. Phys. **64** 481 (1976)

67. Kebarle, P., Ann. Rev. Phys. Chem. **28** 445 (1977)

68. Slater, J. C. & Kirkwood, J. G., Phys. Rev. **37** 682 (1931)

69. Labik, S., Mol. Phys. **64** 21 (1988)

70. Lopatho, O. Ya, Mol. Phys. **64** 111 (1988)

71. Lin, S. H., Fujimura, Y., Neusser, H. J. & Schlag, E. W., Multiphoton Spectroscopy of Molecules, Academic Press, Inc., New York (1984)

72. Kasha, M., Discussions Faraday Soc., **9** 14 (1950)

73. Hopkins, J. B., Powers, D. E. & Smalley, R. E., J. Phys. Chem. **85** 3739 (1981)

74. Wanna, J., Manapace, J. A. & Bernstein, E. R., J. Chem. Phys. **85** 1795 (1986)

75. Carrabba, Michael M., Kenny, Jonathan E., Moomaw, William R., Cordes, John, Denton, Mary, J. Phys. Chem. **89** 674 (1985)

76. Hobza, Pavel & Zahradnik, Rudolf , "Weak Intermolecular Interactions in Chemistry and Biology, Studies in Physical and Theoretical Chemistry, Vol **3**, Elsevier, Amsterdam (1980).

77. Wanna, J. & Bernstein, E.R., J. Chem. Phys. **84** 927 (1986)

78. Kari, R.E. & Csizmadia, I. G., J. Chem. Phys. **56** 4337 (1972)

79. Zalewski, E. F., McClure, D. S. & Narva, D. L., J. Chem. Phys. **61** 2964 (1974)

80. Miertus, S., Scrocco, E & Tomasi, J., Chem. Phys. **55** 117 (1981)

81. Miertus, S., Frecer, V. & Majekova, M., J. Mol. Struct. (Theochem) **179** 353 (1988)

82. Constanciel, R. & Tapia, O., Theoret. Chim. Acta. (Berl) **48** 75 (1978)

83. Jacobs, T. A., Giedt, R. R. & Cohen, N., J. Chem. Phys. **43** 3688 (1965)

84. Lamborelle, C. & Tapia, O., Chem. Phys. **42** 24 (1979)

85. Purvis, G. D. III, & Zerner, M. C. (Unpublished results)

86. Mikkelsen, Kurt V., Agren, Hans, Jensen, Hans Horgen Aa., & Helgaker, Trygve, J. Chem. Phys. **89** 3086 (1988)

87. Morter, Cheryl L., Koskelo, Aaron, Wu, Yenchune R. & Levy, Donald H., J. Chem. Phys. **89** 1867 (1988).

BIOGRAPHICAL SKETCH

The author was born in Colombo, Sri Lanka.

I certify that I have read this study and that in my opinion it conforms to acceptable standards of scholarly presentation and is fully adequate, in scope and quality, as a dissertation for the degree of Doctor of Philosophy.

Michael C. Zerner, Chairman
Professor of Chemistry and Physics

I certify that I have read this study and that in my opinion it conforms to acceptable standards of scholarly presentation and is fully adequate, in scope and quality, as a dissertation for the degree of Doctor of Philosophy.

Willis B. Person
Professor of Chemistry

I certify that I have read this study and that in my opinion it conforms to acceptable standards of scholarly presentation and is fully adequate, in scope and quality, as a dissertation for the degree of Doctor of Philosophy.

N. Yngve Öhrn
Professor of Chemistry and Physics

I certify that I have read this study and that in my opinion it conforms to acceptable standards of scholarly presentation and is fully adequate, in scope and quality, as a dissertation for the degree of Doctor of Philosophy.

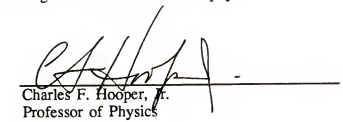

Charles F. Hooper, Jr.
Professor of Physics

I certify that I have read this study and that in my opinion it conforms to acceptable standards of scholarly presentation and is fully adequate, in scope and quality, as a dissertation for the degree of Doctor of Philosophy.

Zoran R. Pop Stojanovic
Professor of Mathematics

This dissertation was submitted to the Graduate Faculty of the Department of Chemistry in the College of Liberal Arts and Sciences and the the Graduate School, and was accepted as partial fulfillment of the requirements for the degree of Doctor of Philosophy.

May, 1989

Dean, Graduate School